Journal of Power Sources 599 (2024) 234211

Contents lists available at ScienceDirect

Journal of Power Sources

journal homepage: www.elsevier.com/locate/jpowsour

Review article

Mitigating thermal expansion effects in solid oxide fuel cell cathodes: A critical review

Nilam Shah [a], Xiaoyong Xu [b,**], Jonathan Love [c], Hao Wang [d,e], Zhonghua Zhu [a,***], Lei Ge [d,e,*]

[a] School of Chemical Engineering, The University of Queensland, Brisbane, 4072, QLD, Australia
[b] School of Chemical Engineering, University of Adelaide, Adelaide, 5000, SA, Australia
[c] School of Chemistry & Physics, Queensland University of Technology, Brisbane, 4001, QLD, Australia
[d] Centre for Future Materials, University of Southern Queensland, Springfield, QLD, 4300, Australia
[e] School of Engineering, University of Southern Queensland, Springfield, QLD, 4300, Australia

HIGHLIGHTS

- SOFCs face performance and stability challenges.
- The review focuses on cathode delamination issue by material design.
- Strategies are reviewed to reduce cathode thermal expansion and delamination.
- Future research opportunities are highlighted.

GRAPHICAL ABSTRACT

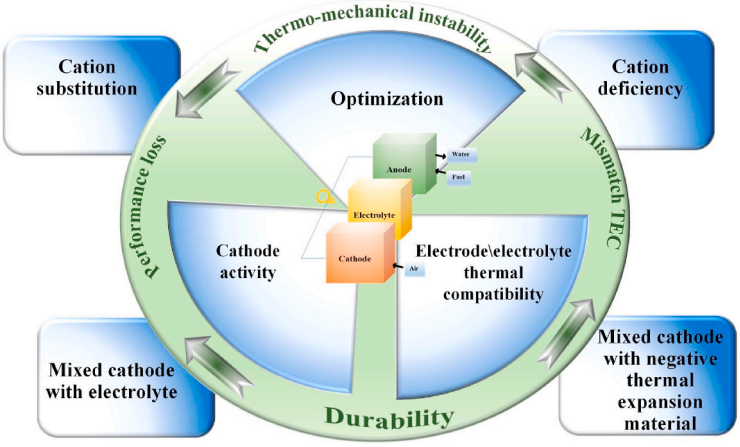

ARTICLE INFO

Keywords:
Solid oxide fuel cell (SOFC)
Thermal incompatibility
Delamination
Cathode materials
Thermal expansion coefficient

ABSTRACT

Solid oxide fuel cells (SOFCs) are a promising technology for clean electricity generation. However, their performance degradation over time and with thermal cycles due to thermal incompatibility remains a significant challenge in achieving the industrial scale. Designing a thermally compatible cathode material to overcome this issue is essential to withstand more thermal cycles. Rather than reviewing the cathode materials, this review critically examines recent advances in mitigating cathode/electrolyte thermal incompatibility and delamination via designing cathode materials and cathode-electrolyte interfaces. This critical review provides an overview of SOFC application, significant challenges, and the delamination mechanism, followed by an elaboration on experimental strategies to tailor the thermal expansion of cathodes to reduce or eliminate cathode delamination.

* Corresponding author.School of Chemical Engineering, The University of Queensland, Brisbane, 4072, QLD, Australia.
** Corresponding author.
*** Corresponding author.
E-mail addresses: xiaoyong.xu@adelaide.edu.au (X. Xu), z.zhu@uq.edu.au (Z. Zhu), lei.ge@usq.edu.au (L. Ge).

https://doi.org/10.1016/j.jpowsour.2024.234211
Received 19 December 2023; Received in revised form 10 February 2024; Accepted 13 February 2024
Available online 19 February 2024

In the last section, the remaining challenges and future research opportunities are discussed to support the design of thermally compatible cathode materials for SOFCs with high durability.

1. Introduction

The rise in energy consumption across various aspects of human life results in an urgent need for high-efficiency green energy solutions with less harmful emissions. Solid Oxide Fuel Cells (SOFCs) achieve higher efficiency than other gas-to-power and heat technologies and have the potential to be one of the future energy solutions [1]. As presented by the U.S. Department of Energy [2], the commercialization and increased use of SOFC products will reduce its capital cost and minimize the production of gas emissions. Fuel cells can be classified into various categories based on the electrolytes used, and solid electrolyte-based SOFCs offer greater efficiency and additional benefits such as fuel flexibility and lower emissions due to high-temperature operation [3,4]. This power and heat generation technology can be used in residential

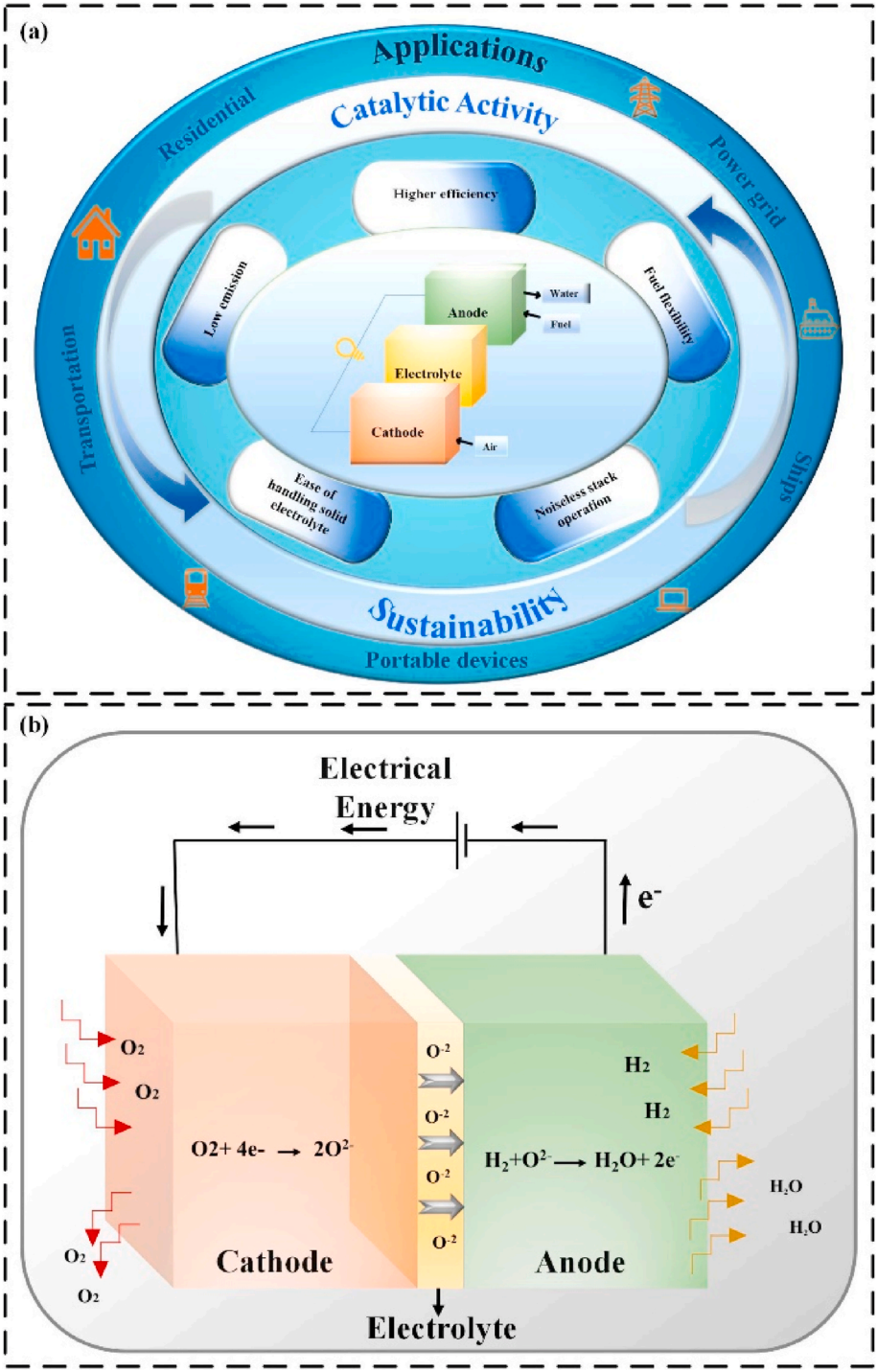

Fig. 1. (a) Illustration of SOFC as a versatile, sustainable energy generator (b) Working mechanism of SOFC with hydrogen as the fuel.

and industrial applications, as shown in Fig. 1a, and can be customized for different electrical applications by varying the stack size. This is a distinctive feature of SOFCs that makes them highly versatile.

A solid oxide fuel cell (SOFC) is a stationary power and heat generation device that directly transforms the chemical energy of a fuel into electrical and heat energy through an electrochemical reaction [5,6]. A piece of fuel cell comprises three main functional layers - anode, electrolyte, and cathode - arranged in series. Depending on the application and power requirement, individual cells can be connected in series by connecting the cathode of one cell to the anode of another cell through gas impermeable interconnectors. The working principle of a SOFC is shown in Fig. 1b. Oxygen molecules in air are reduced at the cathode into oxygen ions, that are transferred to the anode through the solid oxide electrolyte. At the anode the oxygen ions oxidise the fuel that generates free electrons. When individual cells are stacked in series, the electrons conduct through the interconnector from the anode to the cathode of the next cell. The generated electrons flow to an external electrical circuit, creating electricity for use, and return to the cathode, where the same process is repeated. Unlike batteries, SOFCs operate continuously when the fuel and air are continuously supplied.

SOFCs offer a range of benefits as a cleaner energy solution, including higher efficiency of up to 90% when used in a combined heat and power (CHP) application, with high power to heat ratio up to 2.5, fuel flexibility allowing for various fuel options, and a solid oxide electrolyte that protects the system from corrosion and electrolyte loss [6]. However, the commercialization of SOFCs face challenges by insufficient durability and the high capital cost. While mass production can address cost issue through learning rates, the high operation temperature necessitates prolonged start-up time and precise control of operating conditions for high reliability, safety, and durability, leading to added equipment and operating costs. To expedite the commercialization of SOFCs, it is vital to further enhance the durability and reduce the cost without compromising much performance. This can be potentially realized through the strategic operation of SOFC stacks at intermediate temperatures, specifically those below 600 °C.

Operating at lower temperatures can have a negative impact on the performance of SOFC due to several factors, such as slower oxygen reduction reaction (ORR) [7] and fuel oxidation kinetics at cathode and anode, respectively, reduced methane steam reforming capacity, lower electrolyte conductivity, and overall reduced performance. Researchers have conducted numerous studies on intermediate-temperature electrodes and electrolytes to address these issues. For SOFC to operate at intermediate temperatures, a sustainable cathode with higher activity and thermal compatibility is critical to overcome the barrier of sluggish ORR at lower temperatures [8–12]. However, the significant efforts to improve the ORR kinetics of SOFC at reduced temperatures have not overcome this challenge. To address this challenge, various strategies have been explored to produce state-of-the-art cathodes, including preparation of composite cathodes, creation of deficiencies, surface modification, and addition of buffer layers, which have been evaluated for their performance.

The contemporary cathode material in SOFC is Co-based perovskite due to its mixed ionic and electrical conductivity (MIEC), essential for improving electrochemical activity [13,14]. Various cobaltite perovskite materials such as $La_{0.6}Sr_{0.4}Co_{0.2}Fe_{0.8}O_{3-\delta}$ [15], $La_{0.6}Sr_{0.4}Co_{0.2}Fe_{0.8}O_{3-\delta}/CeO_2$ [16], $La_{0.6}Sr_{0.4}Co_{0.2}Fe_{0.8}O_{3-\delta}$ by surface modification [17], $Ba_{0.5}Sr_{0.5}Co_{0.8}Fe_{0.2}O_{3-\delta}$ [18], $Ba_{0.5}Sr_{0.5}Co_{0.8}Fe_{0.2}O_{3-\delta}$ with high specific area [19], and $SrCo_{0.8}Nb_{0.1}Ta_{0.1}O_{3-\delta}$ [20], $SrCo_{0.8}Sc_{0.175}Ta_{0.025}O_{3-\delta}$ [21,22] with synergistic substitution, $La_{0.6-x}M_xSr_{0.4}Co_{0.2}Fe_{0.8}O_3$ (M = Ca, Ba, Bi; x = 0, 0.1, 0.2) [23], $SrCo_{0.8}Ti_{0.1}Ta_{0.1}O_{3-\delta}$ [24], $SrNb_{0.1}Co_{0.9}O_{3-\delta}$ [25] etc. have shown improved performance and gained considerable attention among scientists. The high performance of cobaltite perovskite material as a cathode in SOFC is unequivocal, but the major challenges faced by these materials are the stability of the crystal structure of cobaltite materials below 900 °C [26], susceptibility towards contaminants [27], and thermal expansion mismatch with internal components. Cobalt undergoes a spin state change at high operating temperatures, resulting in a significant difference in thermal expansion coefficient (TEC) values between cobaltite perovskite cathodes (20–26) $*10^{-6}$ K^{-1} and other components, such as the electrolyte material and interconnectors (10–13) $*10^{-6}$ K^{-1}. It is critical that the cathode is strongly connected to the electrolyte throughout the operating life of the SOFC to maintain high performance of the ORR. High thermal gradients experienced by SOFC cells generate significant thermomechanical stress between these thermally mismatched components and the resulted thermo-mechanical shock can cause detachment between layers, leading to significant performance degradation that may be rapid and catastrophic.

Several review articles have provided a comprehensive understanding of cathode materials for SOFC, including their design, surface modification techniques, and approaches to overcome poisoning issues [11,13,28–42]. However, it is also critical to understand and address the challenge of thermal expansion mismatch between cathode and electrolyte materials. Further review of the state-of-art SOFC cathodes is beyond the scope of this article. This review focuses on the cathode delamination mechanism and the design strategies to mitigate thermal expansion incompatibility, which has been underexplored by previous reviews. Section 2 discusses the mechanism of cathode delamination and its impact on performance, while section 3 focuses on the strategies to reduce the rate of delamination and improve SOFC sustainability by targeting the thermal expansion mismatch of internal components. The review concludes with a summary of findings and perspectives for future research in the last section.

2. Mechanism for cathode delamination

In the complex structure of SOFCs, the nuanced issue of thermal expansion mismatch between emerging cathode materials and conventional electrolytes reveals its impact on structural integrity and long-term performance. Thermal expansion mismatch is a fundamental factor contributing to delamination in solid oxide fuel cells (SOFCs). Delamination manifests when there is a disparity in the thermal expansion behaviour between the cathode and electrolyte layers of an SOFC during temperature changes. This discrepancy leads to the generation of thermomechanical stresses at the interfaces between these layers. Fundamental understanding of the mechanisms behind thermal expansion mismatch is essential for implementing effective strategies to mitigate delamination and enhance the long-term performance and durability of SOFCs.

Some of the most promising cathode materials may not withstand practical applications due to their higher TEC at operating temperatures than the TEC of traditionally used electrolytes. For example, the detachment between the cathode and electrolyte has been illustrated in the literature through a single cell using LSM as the cathode [43]. Fig. 2 demonstrates the impact of crack formation at the interface of cathode and electrolyte. When the cathode delaminates from the electrolyte, ion transfer can be obstructed, and the ORR is disrupted. This interference results in a decline in fuel cell performance over time due to degradation. The degradation in SOFC performance attributed to cathode delamination has also been investigated and demonstrated in single-cell SOFCs utilizing PSCF as cathode [44], where a detachment of interfaces was observed when the TEC difference between the cathode and electrolyte was high. Additionally, research has demonstrated that detachment of electrodes from electrolytes leads to an elevation in polarization resistance and ohmic losses. Consequently, this phenomenon contributes to a reduction in power density. The delamination issue significantly accelerates system degradation compared to other degradation mechanisms, such as grain growth. Although various promising MIEC cathodes show adequate electrochemical behaviour, they have higher TEC than commonly used electrolytes such as YSZ (yttria-stabilized zirconia), SDC (Samaria doped ceria), and GDC. Table 1 provides examples of promising cathodes and electrolytes, along with their respective TEC values.

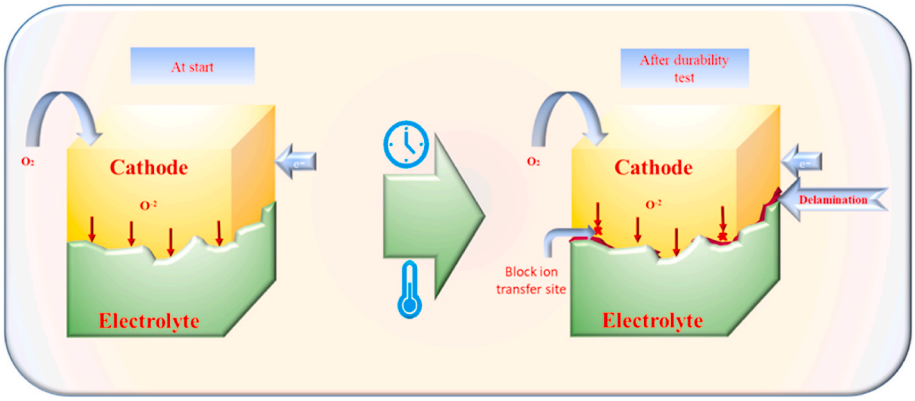

Fig. 2. Illustration of the delamination of the cathode from an electrolyte.

Table 1
TEC value for promising cathodes and electrolyte materials.

Composition	Material	TEC (* 10^{-6} K^{-1})	References
Cathode	BSCF	24.9	[45]
Cathode	LSCF	19.5–20.5	[46,47]
Cathode	SNC	20.5	[48]
Cathode	SSNC	21.4–23.8	[49]
Cathode	SSTC	25.87	[21]
Cathode	SCNT	26.27	[50]
Electrolyte	SDC	12.44	[51]
Electrolyte	YSZ	10.0	[52]
Electrolyte	GDC	12.5	[52]

The TEC values reported in the literature revealed that, the TEC of the promising cathode material BSCF is almost twice that of the electrolyte SDC. This high TEC, ascribe to an increase in the ionic radii of cobalt ions at operating temperatures, poses a challenge to the durability of SOFCs due to thermo-mechanical failure. Despite BSCF's good electronic and ionic conductivity, its high TEC is a limiting factor. The determination of TEC involves various parameters, such as the thermal behaviour of the BO_6 octahedron, octahedral tilt, distortion, and bonding between the B-site cation and anion [53]. These factors collectively influence the TEC measurement, which depends on compositional changes and electronic and magnetic transitions at operating temperatures [34]. Additionally, the operating temperature significantly affects the TEC value, as evidenced by the increase in TEC of $Sc_{0.75}Y_{0.25}Fe_{0.75}Co_{0.25}O_{3-\delta}$ from 14.6 $\times$ 10^{-6} K^{-1} to 22.1 $\times$ 10^{-6} K^{-1} at temperatures above 400 °C [54]. This emphasizes the sensitivity of TEC to temperature variations and underscores its importance in assessing material suitability for SOFC applications.

Strontium-cobaltite (SC) type perovskite material stands out for having the highest ionic conductivity and TEC values among the cathode materials studied, but its high TEC restraints its applicability. Researchers have attempted to reduce the TEC by substituting strontium and cobalt; however, this approach diminishes both the electric and ionic conductivity, leading to unsatisfactory electrochemical behaviour. An alternative strategy involves the use of a composite cathode to enhance electrochemical performance, provided that the electrolyte material is added judiciously. For instance, adding 50% SDC to $Gd_{0.8}Sr_{0.2}CoO_{3-\delta}$ (GSC) reduces its TEC from 24.84 $\times$ 10^{-6} K^{-1} to 13.38 $\times$ 10^{-6} K^{-1}, which is close to the TEC of SDC electrolyte. However, this 50% addition doubles the value of area specific resistance (ASR) from that of GSC alone. This outcome suggests that an excessive addition of electrolyte may be disadvantageous [51]. Finding the right balance in composite cathode formulations is crucial for optimizing both TEC and electrochemical performance in solid oxide fuel cell applications.

BSCF and LSCF emerge as the most promising *SC*-type cathodes due to their high conductivity, low polarization resistance, and high-power density, and they have gone under extensive investigation for their electrochemical properties at intermediate temperatures. However, despite their positive attributes, their commercial viability is hindered by high TEC values. This is particularly problematic as their TEC does not align with the commonly used electrolytes, such as SDC, at intermediate temperatures.

For SOFCs to become a commercially viable energy-generating option, there is a need for a cathode material that not only exhibits a TEC closer to that of the electrolyte but also demonstrates improved ORR kinetics and enhanced durability. Numerous studies have been conducted to address the challenge of reducing the TEC of cathodes, yet the development of a cathode material meeting all these criteria remains an ongoing pursuit. The quest for a cathode that achieves the right balance of TEC compatibility, ORR kinetics, and durability is crucial for advancing the commercialization of SOFCs in practical energy applications.

3. Strategies applied to offset thermal expansion of cathode

To prevent the degradation of SOFC due to cathode delamination, it is necessary to adjust the TEC of the cathode to match that of the electrolyte, either by modifying existing cathodes or designing new ones. By reducing the difference in TEC between the two components and minimizing sudden expansion at operating temperatures, thermomechanical stress on the system can be reduced, ultimately improving the sustainability of the system. Four approaches have been taken to adjust TEC, including A-site or B-site substitution to tailor TEC, creating A-site deficiencies, tuning electrolyte contents in composite cathodes, and adding negative thermal expansion (NTE) materials to the cathode.

3.1. Cation substitution

Cation substitution has been explored as a promising strategy to tailor the TEC of SOFC cathodes and enhance their structural stability. In this section, we delve into the intricacies of A-site or B-site doping, examining its impact on TEC, electrochemical behaviour, and overall performance. Doping another cation on A-site or B-site can be used to develop a range of materials with optimized properties, including improved oxygen reduction reaction (ORR) activity, TEC tailoring, and structural stability. However, in some cases, improving one property may compromise the performance of another. For example, substituting strontium and/or cobalt can reduce TEC but also decrease the electrochemical capabilities of the cathode, increasing polarization and ohmic resistance and reducing power density. The strategic choice of doping elements is pivotal in navigating this trade-off. Significance of the doping strategy is well presented for $Ba_{0.5}Sr_{0.5}Co_{0.8}Fe_{0.2}O_{3-\delta}$ (BSCF) and how A-site doping can improve structural stability by doping with lanthanum and provide chemical stability via less deformation in cubic

symmetry under operating conditions of SOFC [55]. This underscores the intricate balance required in the doping process to optimize multiple material properties for improved overall performance in SOFC applications.

To develop an optimal solution, it is essential to pursue comparable, or better, electrochemical behaviour and align the TEC of the cathode to that of the electrolyte. The impact of lanthanide A-site doping on the TEC behaviour and electrochemical properties has been investigated in a recent study [56]. The findings of this study are depicted in Fig. 3. The investigation affirms that A-site doping with lanthanides reduces the TEC value significantly compared to strontium and cobalt-rich perovskite material. In the context of optimizing simultaneously thermal expansion behaviour and electrochemical behaviour, praseodymium (Pr) doping emerges as particularly effective. The Pr doping achieved an ASR of 0.038 and 0.026 Ωcm^2 and peak power densities of 905.9 and 1236.4 $mWcm^{-2}$ at temperatures of 650 and 700 °C, respectively. The highest measured TEC value was found to be $16.2 \times 10^{-6}\ K^{-1}$, spanning the temperature range from room temperature to 800 °C under ambient conditions. Furthermore, this cathode material exhibited stability over a period of 150 h, indicating consistent and reliable performance. Similar findings were observed, which demonstrated that substituting Sr with Pr can generate more oxygen vacancies due to the availability of multiple oxygen adsorption sites, resulting in higher ionic conductivity than *S*C-type perovskites [57].

Numerous examples in the literature showcase the positive outcomes of A-site doping with lanthanides, highlighting their excellent behaviour. For instance, the effect of different lanthanide dopants on A-site in $Ln_{0.3}Sr_{0.7}Fe_{0.7}Cr_{0.3}O_{3-\delta}$ (Ln = La, Pr, Nd, Sm) was evaluated for their electrochemical behaviour and TEC value [58]. The study highlights that adjusting TEC for the low-temperature range can be achieved by

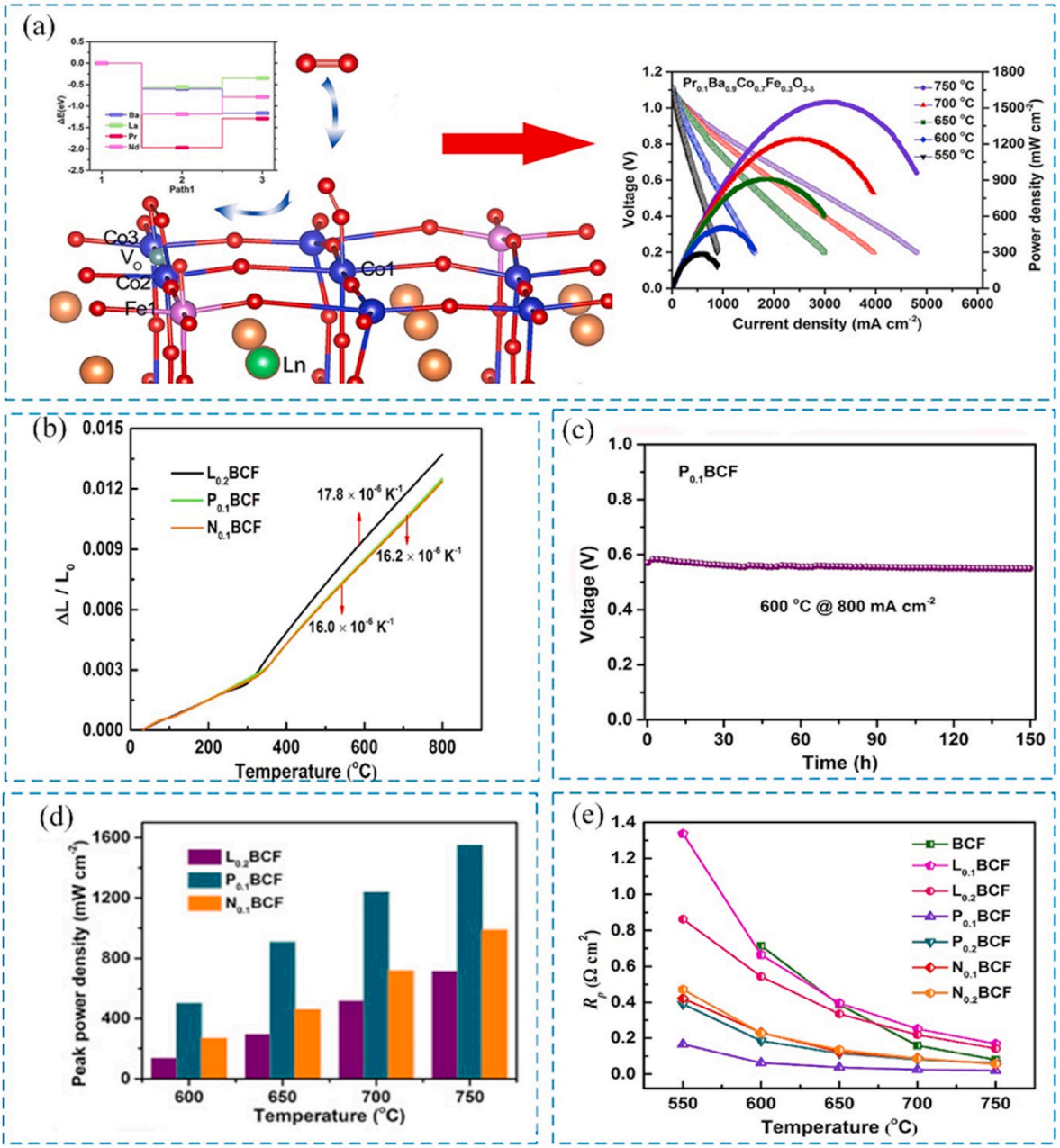

Fig. 3. (a) Schematic illustration of A-site doping with lanthanides and effect on power density (b) Thermal expansion behaviour from room temperature to 800 °C in air for $Ln_xBa_{1-x}Co_{0.7}Fe_{0.3}O_{3-\delta}$(Ln = La, Pr, Nd (c) stability test result for Pr doped BCF (d) power density for $Ln_xBa_{1-x}Co_{0.7}Fe_{0.3}O_{3-\delta}$(Ln = La, Pr, Nd) with respect to temperature (e) Temperature dependence of ASR for $Ln_xBa_{1-x}Co_{0.7}Fe_{0.3}O_{3-\delta}$(Ln = La, Pr, Nd) Reproduced with permission [56]. Copyright 2019, Elsevier.

reducing the size of the lanthanide cation. This reduction induces increased structural deformation and decreased dimensions of primitive unit cells in perovskite structures. Simultaneously, there is a slight rise in the oxygen deficiencies of these perovskites at elevated temperatures. The electrical conductivity of these perovskites consistently decreases with diminishing lanthanide cation sizes, leading to a reduction in their thermal expansion coefficients (TECs), especially below ~600 °C. $Sm_{0.3}Sr_{0.7}Fe_{0.7}Cr_{0.3}O_{3-\delta}$ (SSFCr) emerges as the optimal composition, exhibiting a favourable combination of properties, including an average TEC aligned with IT-SOFC electrolytes, satisfactory electrical conductivity, and commendable electrocatalytic activity. This study highlights the efficacy of lanthanide replacement in optimizing the overall properties of chromium ferrite cathode materials, emphasizing the potential of cobalt-free perovskite compositions like SSFCr for use in IT-SOFC cathodes. A balance between electrochemical behaviour and TEC can be achieved by doping with samarium (Sm). However, it is noted that reducing the lanthanide cation size deforms the structure and adversely impacts the electrochemical activity. Additionally, the effect of substituting strontium with an alkaline earth metal on thermal expansion was observed and explained in Ref. [59], where the effect of barium content in $Ba_xSr_{1-x}Co_{0.8}Fe_{0.2}O_{3-\delta}$ on TEC was evaluated. The study found that substituting strontium with barium had a negligible effect on TEC, while electrical conductivity decreased significantly with an increase in barium content and a decrease in strontium content. The authors suggested that perovskites with 40–50 mol% barium content could be promising cathode materials for further research.

Furthermore, B- site substitution can involve transition metals such as Fe, Mn, Ni, Cu, etc. The study presented in Ref. [60] showed through thermogravimetry analysis that an increase in the valence of the substitutional cation leads to higher oxygen content (3–δ) and enhances the stability of the perovskite structure. Additionally, existing literature supports the idea that high valence doping maintains the stability of cubic symmetry [61]. The comparison between the perovskite stability sequence and oxygen permeability suggests that these factors are not mutually exclusive. In this study, $Sr(Co_{0.9}X_{0.1})O_{3-\delta}$ where X was Ni, Cu, Zn, Cr, Fe, Al, Ga, In, Ce, Ti, Zr, Sn, V, and Nb were investigated for the stability of the perovskite structure, finding that the sequence of the stability of the perovskite with substitution in SC was as follows:

Ni, Cu, Zn, In, Ce < Cr, Al, Ga, Zr, Sn, V < La < Fe < Ti < Nb

Iron (Fe) is a frequently used dopant for *S*C-type oxides; found in state-of-the-art cathodes like LSCF, and BSCF. The Substitution of cobalt (Co) by Fe may increase the stability of the structure and reduce TEC, but unfortunately, it also reduces oxygen vacancies, and accordingly, the conductivity of the material also decreases as Fe content increases. The higher TEC of cobalt-based cathode materials is attributed to the spin transition of cobalt from a low spin state to a high spin state (LS-HS) at higher temperatures [62]. Along with the stability of the structure electroactivity of the material also plays an important role in achieving optimum performance. The electroactivity of the material is likely influenced by an ORR-related properties, such as bulk oxygen ionic conductivity and oxygen surface-exchange kinetics [63]. The ionic conductivity, determined by factors like lattice geometry, critical radius [64], and available lattice free - volume for oxygen ions [65], significantly affects the electrochemical behaviour. Also, material compatibility is a crucial aspect influencing electrochemical stability. Moreover, the presence of oxygen vacancies has been shown to alter the TEC of the material [66]. Chemical expansion at elevated temperatures may be more closely related to B-site element characteristics and the number of oxygen vacancies [67]. Usually, The TEC curves gradually increase with temperature and deviate from linearity from the low (RT-400 °C) to high temperature (400–800 °C) regions. The observed inflection point at high temperatures might be due to the loss of lattice oxygen [68].

Recently nano composites $BaCo_{1-x}Zr_xO_{3-\delta}$(X = 0.2–0.8) have been evaluated [69] for promising material as cathode for intermediate and low-temperature SOFC operation. As depicted in Fig. 4b, this material can tune TEC with 40% substitution of cobalt by zirconium to match the TEC range of the electrolyte. However, it increases the value of ASR and decreases peak power density in the temperature range of 650–800 °C as presented in Fig. 4f. Electrochemical studies at lower temperature confirms similar or slightly better results for ASR (Fig. 4 d & e) and Peak Power Density (PPD) (Fig. 4g) in the temperature range of 500–600 °C. At 40% substitution of cobalt with zirconium achieved value of ASR is 1.372 and 2.430 Ω cm^2 at 550 and 500 °C respectively. The nanocomposite and its designing process which is presented in Fig. 4a can form heterointerfaces that enhance the overall ORR activity and enable operation at low and intermediate temperatures.

The effect of cobalt substitution on thermal expansion was investigated by substituting cobalt at different percentages in $Nd_{0.8}Sr_{0.2}Co_{1-y}Fe_yO_{3-\delta}$ [70]. The findings suggest that substituting cobalt with iron can eliminate cobalt from the structure, achieving a thermal expansion coefficient (TEC) value closer to that of the electrolyte. However, this substitution may concurrently increase the polarization resistance of the cathode, as demonstrated in a study on the BSCF cathode [71], where an EIS study was performed on BSCF at different cobalt substitution levels. The study on BSCF showed that substituting cobalt by more than 20% results in an increase in polarization resistance. Moreover, it was confirmed that reducing TEC at 20% cobalt substitution did not yield the anticipated TEC results. The reduction of TEC through B-site cobalt substitution has been explored in various studies. Examples include cobalt substitution with Mn and Fe [72], computational theory presented for substitution of Co with other metals such as Mn, Fe, Ni, Cu [73], B-site Fe doped $YBa_{0.5}Sr_{0.5}Co_{2-x}Fe_xO_{5+\delta}$ [74], A-site-deficient Ti-doped SrCoO3-δ (SCT) [75], cerium doped $Sm_xSr_{1-x}CoO_{3-\delta}$ [76], etc. Researchers have recently explored B-site doping of Fe in the cathode material $La_{0.6}Sr_{0.4}Co_{0.2}Fe_{0.8-x}M_xO_3$ (M = Ni, Cu, Nb; x = 0, 0.1, 0.2) [77]. The study reveals that Cu doping in $La_{0.6}Sr_{0.4}Co_{0.2}Fe_{0.8-0.1}Cu_{0.1}$ (LSCFC) cathodes reduces the Thermal Expansion Coefficient (TEC) in $La_{0.6}Sr_{0.4}Co_{0.2}Fe_{0.7}Cu_{0.1}$. However, in $La_{0.6}Sr_{0.4}Co_{0.2}Fe_{0.7}Cu_{0.2}$, an intermediate TEC below 550 °C is observed, attributed to a balance between increased oxygen vacancies and reduced crystal volume, while surpassing others above 550 °C due to the lower bond energy of Cu - O.

Although the strategy of substituting other cations in A and B site in SC perovskites can help to mitigate the TEC mismatch issue, researchers have explored alternative approaches to provide a solution with comparable electrochemical behaviour, which are explained in the following sections.

3.2. Cation deficiency

Exploring the strategic deployment of A-site deficiency in perovskite structures, this section investigates its transformative impact on the physical and chemical characteristics. Emphasis is placed on its application in mitigating thermal expansion in cathode materials for enhanced performance in fuel cells. The creation of A-site deficiency is a well-known technique for introducing A-site non-stoichiometry in the defect-free ABO_3 perovskite structure, which can modify the physical and chemical properties. This approach has been extensively explored in the literature, leading to favourable outcomes [78–80]. Recently, researchers have leveraged A-site deficiency to facilitate the exsolution of B-site, generating oxygen vacancies that drive phase stabilization from non-stoichiometric to defect-free perovskite structure [81–86]. Several studies in the literature have proposed that A-site deficiency can effectively enhance electrochemical activity [78,87,88]. However, there is limited research on utilizing this approach to reduce the thermal expansion of cathode materials. BSCF is widely known for its exceptional electrochemical characteristics, but its high coefficient of thermal expansion (TEC) and the consequent decrease in ORR activity during thermal cycles have been significant challenges. Fig. 5 illustrates the investigation conducted on A-site deficient $(B_{0.5}S_{0.5})_{1-x}C_{0.8}F_{0.2}O_{3-\delta}$ (x = 0.03–0.2), evaluating their thermal and electrochemical performance.

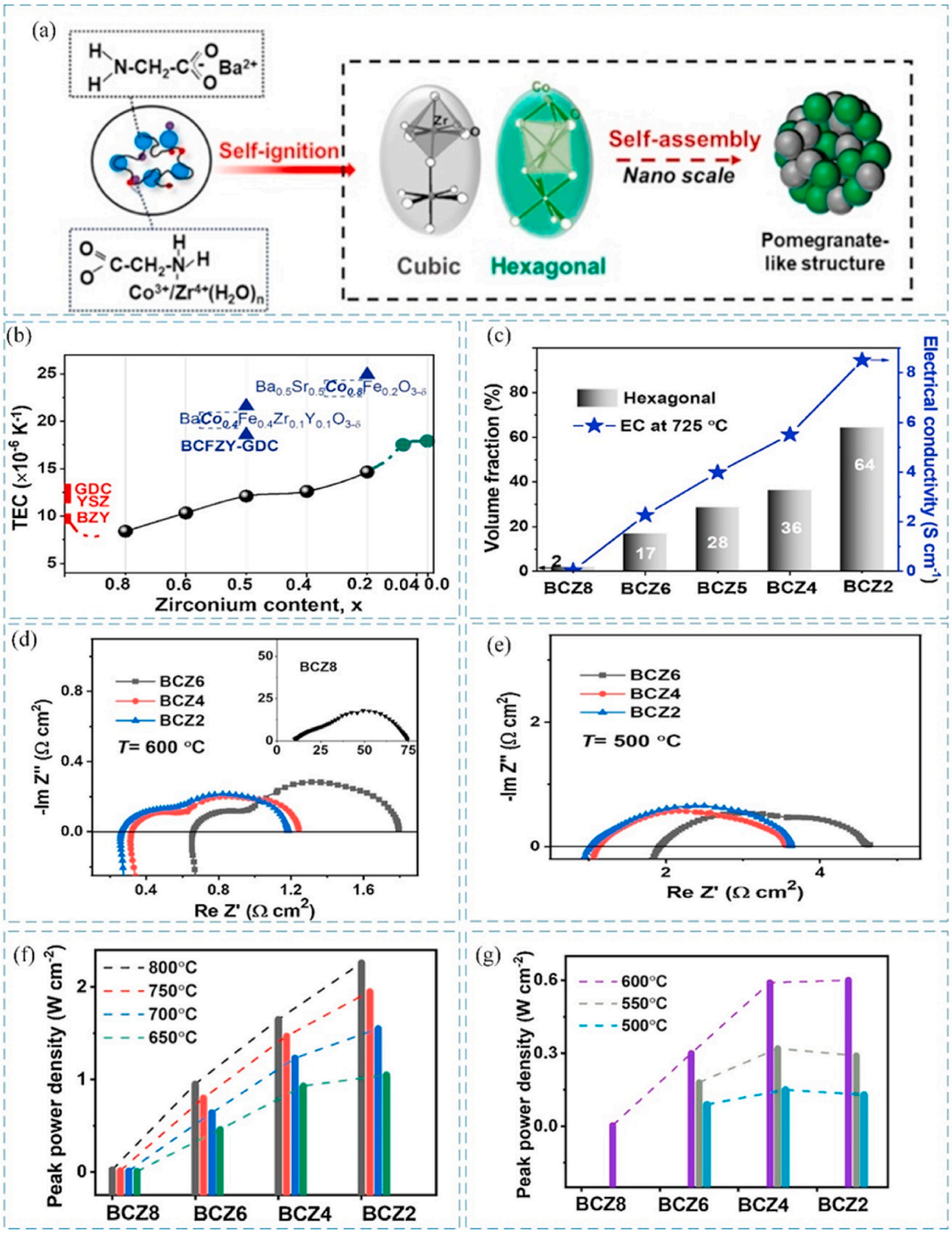

Fig. 4. (a) The diagram of rationally designed $BaCo_{1-x}Zr_xO_{3-\delta}$ nano composites via self-assembled process (b) TEC of $BaCo_{1-x}Zr_xO_{3-\delta}$ with respect to zirconium content, The electrochemical spectra of $BaCo_{1-x}Zr_xO_{3-\delta}$ with (X = 0.2,0.4 and 0.6) at (c) 600 °C and (d) 500 °C, the PPDs of cells tested with $BaCo_{1-x}Zr_xO_{3-\delta}$ (x = 0.8,0.6,0.4,0.2) nanocomposites as cathodes at (e) 800°C–650 °C (f) 600°C–500 °C Reproduced with permission [69]. Copyright 2021, Elsevier.

The researchers observed that A-site deficiency can be incorporated in the BSCF structure within the range of 0.0–0.15, as up to this limit of deficiency, the perovskite structure maintains cubic symmetry, while beyond this limit of deficiency, impurity phases may appear [89]. They also confirmed the shrinking of the perovskite lattice structure in XRD data by the shifting of the main diffraction peak to a higher angle as deficiency increases (Fig. 5c). This structural adjustment was found to reduce the TEC of BSCF. The obtained TEC data for A-site deficient BSCF, showed a significant TEC reduction as A-site deficiency increased, particularly in the temperature range of 450–700 °C (Fig. 5d).

Similar observations were reported for A-site deficient LSCF in previous studies [78,80]. The reduction in TEC in both A-site deficient LSCF and BSCF is attributed to a decrease in lattice parameters and a reduction in oxidation states. Additionally, the suppression of cobalt ion spin

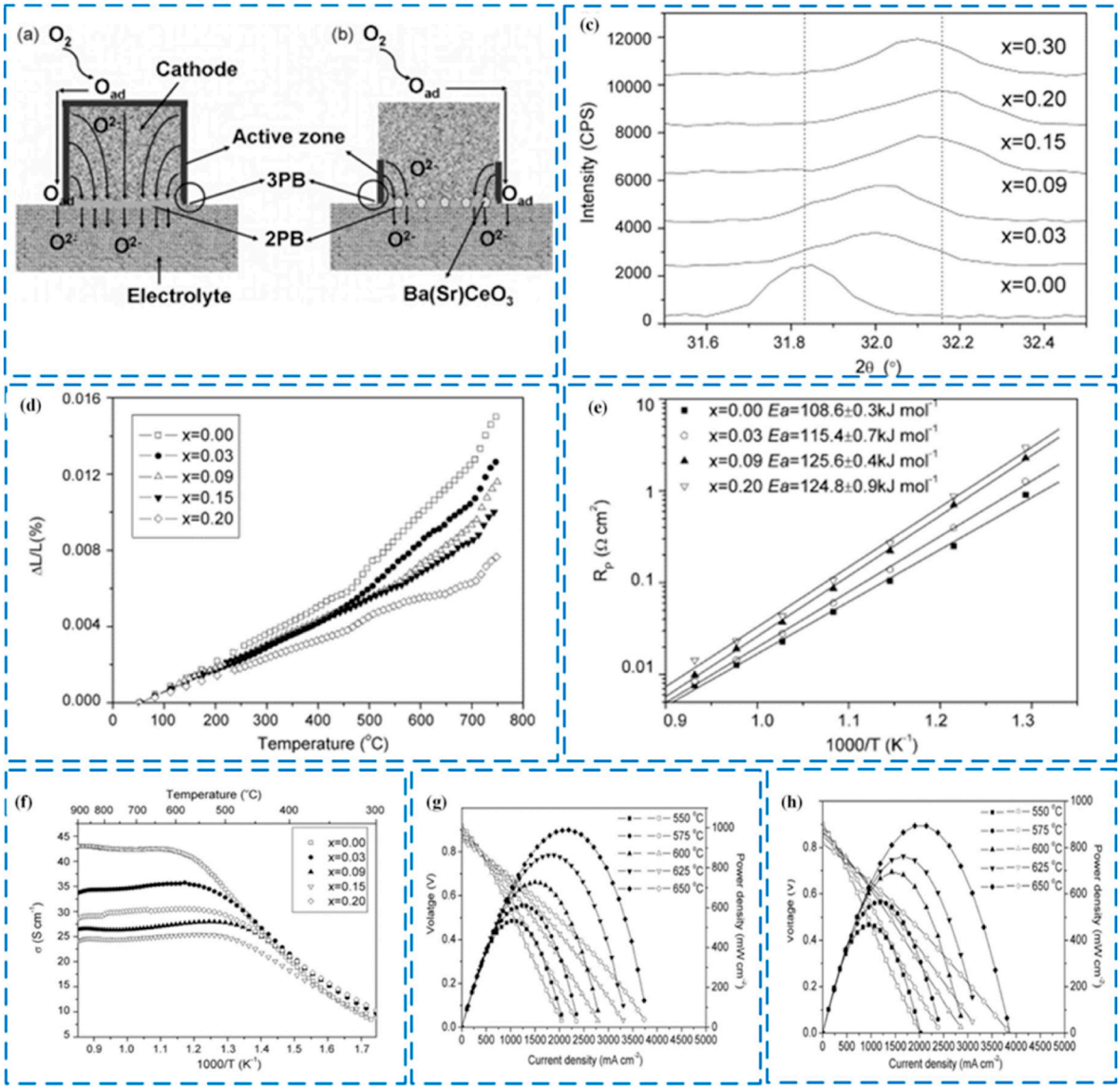

Fig. 5. Schematic of the oxygen reduction reaction with (a) $BS_{0.80}CF$ (b) $BS_{1.20}CF$, showcasing engagement of cathode surface in oxygen reduction (c) XRD patterns for $(BS)_{1-x}CF$ (X = 0.0–0.30) (d) Linear thermal expansion curves for $(BS)_{1-x}CF$ (x = 0.00–0.20) under an air atmosphere (e) Temperature dependence of Rp for $(BS)_{1-x}CF$ (x = 0.00–0.20) cathodes (f) Electrical conductivity of $(BS)_{1-x}CF$ (x = 0.00–0.20) oxides under an air atmosphere (g) I–V and I–W curves for SOFCs with $BS_{1.00}CF$ and (h) $BS_{0.80}CF$ cathodes Reproduced with permission [89]. Copyright 2008, Elsevier.

state transitions contributes to this reduction. However, the trend in electronic conductivity differs between the two cases. In A-site deficient BSCF, electronic conductivity decreases monotonically as deficiency increases, while in A-site deficient LSCF, it increases up to a 5% deficiency level. The difference in trend is due to the improvement in symmetry of the structure. Deficiency creation in LSCF improves the symmetry, resulting in enhanced electronic conductivity, while in BSCF, it does not improve symmetry, leading to a decrease in electronic conductivity. Another factor contributing to the decrease in electronic conductivity is the creation of additional oxygen vacancies. As the deficiency level increases, impurity formation at the cathode-electrolyte interface is observed, resulting in an increase in polarization resistance. In the case of A-site deficient BSCF, the only advantage obtained is TEC reduction. However, a deficiency level of 3% is recommended, which produced peak power densities of 694 and 893 $mWcm^{-2}$ at 600 and 650 °C, respectively, with a TEC value of 18.0 (10^{-6} K^{-1}). The optimal A-site cation deficiency in $BS_{0.8}CF$ demonstrates the enhanced cathode surface involvement in oxygen reduction (Fig. 5a and b).

Double perovskite materials have attracted significant research interest for their promising electrochemical properties and high oxygen non-stoichiometry capacity. PBCO double perovskite has been extensively investigated for its exceptional electrochemical performance [90–92], but its higher TEC ($21.5*10^{-6}$ K^{-6} [93]) compared to conventional electrolytes limits its applicability. To address this limitation, researchers have delved into the strategy of creating additional oxygen vacancies by inducing A-site deficiencies of various cations, as documented in the literature [94–97]. The effect of deficiency creation of different cations Pr^{+3}/Ba^{+2} has been examined, and their comparison has been reported in the context of PBCO cathode [96]. The study revealed that the introduction of different cationic deficiencies has distinct effects on the structure and performance of the material, influenced by the resulting chemical defects. In the case of Pr-deficient material, lattice shrinkage was found to be insignificant, while in Ba-deficient material, it was pronounced due to the larger ionic radius of Ba. Pr deficiency reduced electrical conductivity, while Ba deficiency improved it, owing to different charge compensation mechanisms in both materials. However, each material reduced the ASR and activation energy value of the parent material PBCO. Deficiency creation for Pr was

found to be limited to 8 mol%, beyond which the ASR value increased, thereby deteriorating the cell's output. The conclusion is that generating oxygen vacancies through non-stoichiometry can enhance results. However, excessive vacancies may negatively impact oxygen ion diffusion, forming clusters with negative defects, as detailed in Ref. [98] and their simulation work.

3.3. Mixed cathode with electrolyte material

Introducing the concept of composite cathodes, this section examines the scientific strategy of blending electrolyte materials into perovskite structures. This innovative approach aims to fine-tune thermal expansion coefficients for enhanced electrochemical performance in SOFCs. This approach has prompted researchers to explore various composite pairs and formulations to fine-tune TEC while maintaining optimal performance. The concept of composite cathodes was introduced in 1996 by Juhl et al. [99], who demonstrated the benefits of mixing LSM and YSZ to improve SOFC microstructure and thickness, allowing the cells to operate at lower temperatures. Composite cathodes, which include an electrolyte material phase, exhibit enhanced performance due to the extension of triple-phase boundaries (TPBs), as shown in Fig. 6a for LSM and YSZ composites. This breakthrough provided a significant direction for further research into cathode materials, leading to numerous studies on composite cathodes for different purposes in the last decade. Understanding this strategy is crucial to advancing the field of SOFCs.

The study presented a comprehensive analysis of the impact of electrolyte material addition on the TEC using the BSCN-GDC composite cathode as an example [101]. It was elucidated that while the optimum performance was attained with a 20% GDC addition, achieving the desired TEC necessitated a 40% addition, as depicted in Fig. 6b and c. Interestingly, the study unveiled a noteworthy observation that surpassing 30% GDC content led to an increase in the ASR of the composite cathode, as illustrated in Fig. 6d. This elevation in ASR was attributed to microstructural alterations, characterized by more agglomerated particles and a reduction in the continuous contact between BSCN and GDC particles. Additionally, the study provided insight into the single cell performance using the BSCN-20GDC composite cathode, exemplifying its suitability for application as a cathode in SOFCs, as demonstrated in Fig. 6e. To further understand this strategy, we have included promising cathode examples such as LSCF and BSCF in this review, where the addition of electrolyte material can improve electrochemical activity. SDC and GDC have been widely used electrolyte materials in composite cathodes due to their exceptional behaviour at intermediate and lower temperatures [102]. Most composite cathodes are prepared by mixing electrolyte materials with the base perovskite materials to show improved behaviour. The cathode is deemed functional when its ASR is below 1 Ωcm^2 [103]. LSCF is an extensively investigated as a cathode material, particularly for its performance at intermediate temperatures. In the case of composite cathodes prepared via this method, improved performance has been credited to the extension of the TPB and the outstanding binding between electrode and electrolyte when using SDC and GDC as electrolyte and LSCF as the electrode. It was observed that the LSCF-GDC composite cathode provided the best performance at LSCF-GDC (50 wt%-50 wt%) composition, achieving a power density of 625 $mWcm^{-2}$, while at LSCF-GDC (40 wt%-60 wt%) composition, a power density of 563 $mWcm^{-2}$ was obtained [104,105]. Its noteworthy that the different processing techniques and process parameters can have different effects. Composite cathode achieved an ASR of 0.17 Ωcm^2 at 600 °C for the LSCF-GDC (40 wt%-60 wt%) composition [104]. In 2013, Zhao et al. achieved the best value for ASR of 0.07 Ωcm^2 at 600 °C for the LSCF-GDC composition by impregnating nanoparticles of GDC into LSCF. Researchers showed that the best performance for LSCF-SDC compositions was achieved with 50 wt%-50 wt% composition of LSCF-SDC [106,107]. The composite cathode of LSCF brings dual benefits by reducing TEC of LSCF and enhancing ORR activity by extending the TPB region.

Likewise, BSCF cathode in composition with SDC has been observed for the electrochemical activity of SOEC [108], where the performance of SOEC can be improved by adding 20 wt% SDC to BSCF at intermediate temperature (650 °C–800 °C), while 50 wt% SDC addition deteriorates the outcome. Wang et al. made efforts to optimize the process and processing parameters by creating sol-gel derived composites of BSCF-SDC [109]. They also recorded observations on the one of the processing parameters, firing temperature used to prepare symmetrical cells. These observations highlighted the impact of process and processing parameters on overall performance and demonstrated the potential for composites to improve the results. This Similar phenomenon was found for SOFC with the addition of 50 wt% SDC in GSC cathode that the TEC of cathode can be reduced close to that of electrolyte but simultaneously increase the value of ASR [51].

In conclusion, the incorporation of electrolyte materials into perovskite structures for composite cathodes holds considerable promise in enhancing SOFC performance. The strategic adjustment of TEC is critical, as illustrated by the BSCN-GDC composite cathode study. The optimal electrochemical activity was achieved with 20 wt% GDC addition, while the TEC alignment required 40 wt% GDC, such high loading harms the overall performance of the fuel cell. Achieving a balance between TEC matching and electrochemical behaviour emerges as a crucial consideration for optimal SOFC functionality, signifying a notable progression in the field.

3.4. Addition of NTE material in the cathode material

Revolutionizing cathode materials for SOFCs, a groundbreaking strategy involves creating composite cathodes by blending negative thermal expansion (NTE) materials with conventional cathode components. This scientific approach aims to optimize thermal expansion coefficients for enhanced electrochemical performance in SOFC technology. NTE materials are characterized by their ability to contract upon heating, in contrast to most materials that expand when heated. This phenomenon occurs due to space consumption during lattice vibrations when the material is thermally active, leading to thermal contraction [110]. The working principle of NTE materials is illustrated in Fig. 7a.

An example of the above-mentioned approach was demonstrated in Ref. [48] through the development of a composite cathode by blending $Y_2W_3O_{12}$ (YWO) as NTE with $SrNb_{0.1}Co_{0.9}O_{3-\delta}$ (SNC) as a cathode material. The study demonstrated that the addition of 20 wt% YWO to SNC effectively tailors the TEC to closely match that of SDC electrolyte, resulting in improved electrochemical performance, such as an achieved ASR of 0.041 Ωcm^2 at 600 °C. The addition of 20% YWO was found to be adequate for the desired TEC tailoring in SNC, as depicted in Fig. 7c. XRD analysis revealed the formation of an extra phase contributing to the improved electrochemical behaviour of the material. The composite formation mechanism is comprehensively described and illustrated in reference Fig. 7b. The incorporation of NTE provided an additional advantage by enabling the use of a thicker functional layer of the cathode and improving its electrochemical behaviour, as demonstrated by the data presented in Fig. 7d, which shows the ASR with respect to varying cathode thickness. The delamination mechanism associated with thermal expansion mismatch, and how it can be tailored using composite cathodes, is well explained in Fig. 7e. This phenomenon enhances the material's ability to withstand more thermal cycles, as depicted in Fig. 7f and g for SNC and composite cathodes respectively. The researchers achieved a power density of 817 $mWcm^{-2}$ at 650 °C for a 40 μm thick cathode, demonstrating the effectiveness of this strategy for tailoring TEC, especially when the cathode exhibits chemical compatibility with NTE and the addition of NTE can produce excellent electrochemical behaviour.

In the pursuit of enhancing the performance of proton-conducting solid oxide fuel cells (H–SOFC), researchers explored the utilization of composite cathodes by combining the NTE material $NdMnO_{3-\delta}$(NM) with $Ba_{0.5}Sr_{0.5}FeO_{3-\delta}$(BSF) cathode material [111]. Their investigation

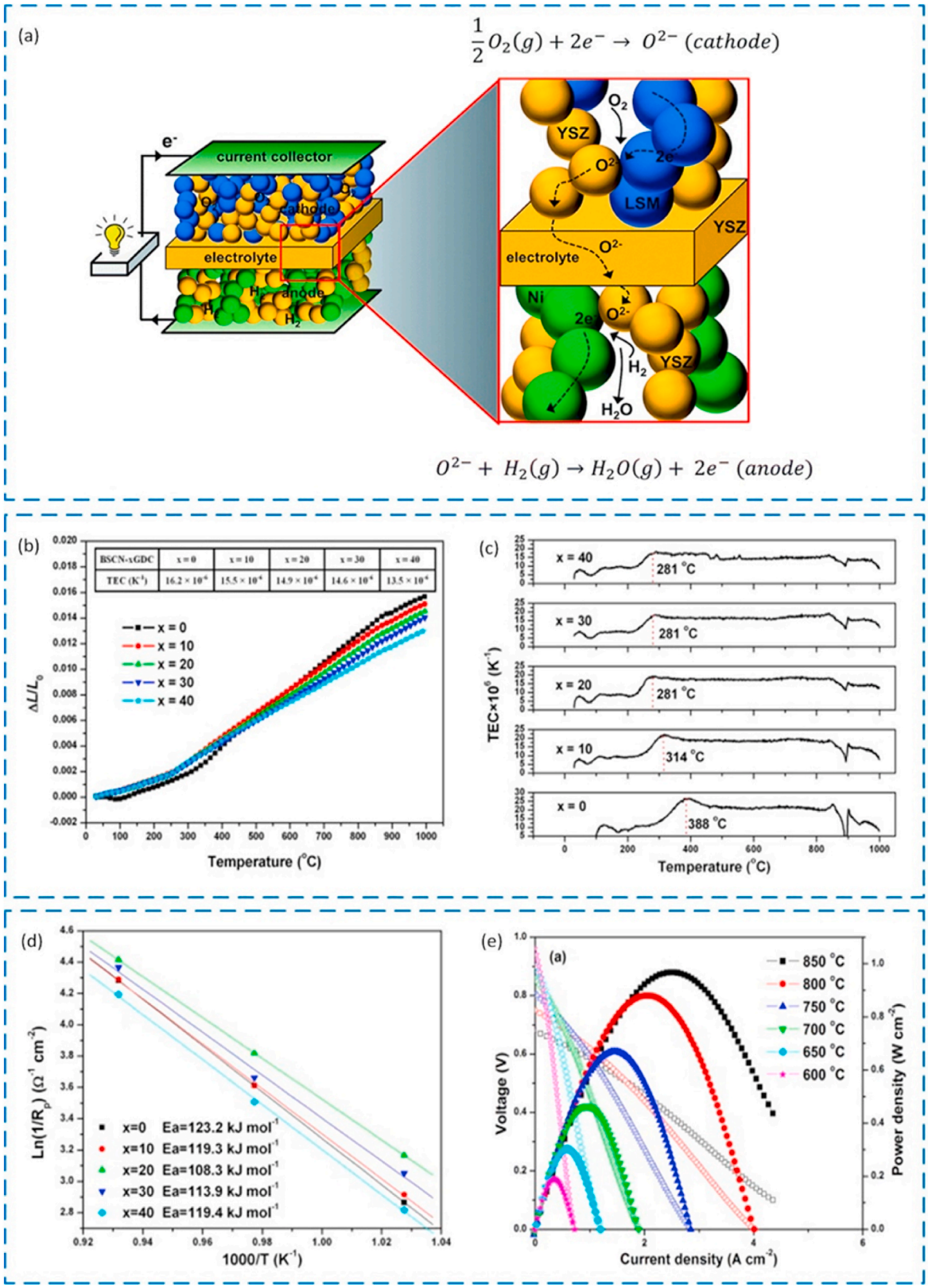

Fig. 6. (a) Working mechanism of the composite electrode by addition of YSZ Reproduced with permission [100]. Copyright 2016, The royal society of chemistry. (b) Thermal expansion and (c) TEC curves of the BSCN-x GDC mixture between 30 and 1000 °C in the air (d) Arrhenius plots for BSCN-xGDC composite cathodes (e) Cell voltage and power density as a function of current density at different temperatures for single cell BSCN-20GDC\GDC\NiO-SDC in H_2 Reproduced with permission [101]. Copyright 2014, Hydrogen Energy.

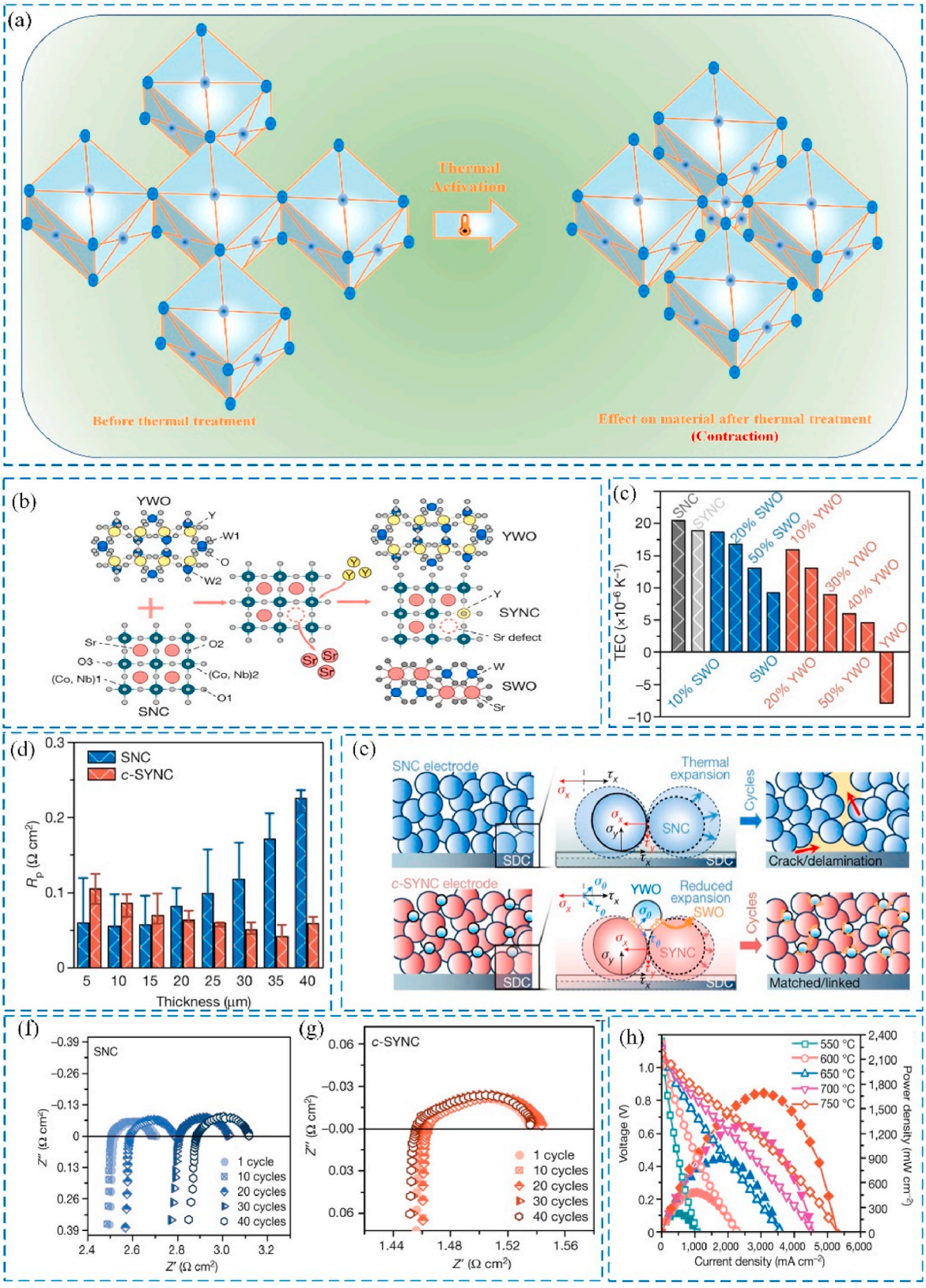

Fig. 7. (a) Working mechanism of NTE materials upon thermal activation (b) Schematic of formation mechanism for c- SYNC (c) TEC measurement of SNC, SYNC, x wt% SWO-SNC and x wt% YWO-SNC composition (d) ASR values for *C*-SYNC and SNC as a function of cathode thickness for symmetric cell configuration (e) Proposed mechanism for thermo-mechanical enhancement by TEC offset (f) & (g) Representative EIS Nyquist plots for the SNC(f) and *C*-SYNC(g) for symmetric cell after cycling (h) The I–V and *P*–I curves of an anode-supported H2/air SOFC with a 40 μm thick c-SYNC cathode Reproduced with permission [48]. Copyright 2021, Springer Nature.

revealed that adding 30 wt% of NM to the composite cathode improved the electrochemical activity and reduced the TEC, bringing it closer to that of the preferred electrolyte $BaZr_{0.1}Ce_{0.7}Y_{0.2}O_{3-\delta}$(BZCY). The researchers achieved a peak power density of 139–941 $mWcm^{-2}$ between 500 and 700 °C, which was higher than that of BSF. A recent study effectively highlights another instance of a composite cathode incorporating the NTE material $Sm_{0.85}Zn_{0.1}5MnO_3$ (SZM) into SNC cathode. In this research, an impressive TEC value of $13.74*10^{-6}$ K^{-1} and a remarkable ASR value of 0.012Ωcm2 at 700 °C were achieved [112]. The subsequent section provides details on the selection criteria and suitable materials for utilizing various NTE materials to tailor the TEC of cathode materials.

However, despite this promising approach, certain cathodes have higher TEC than SNC, which may require a higher addition of NTE and may result in a deterioration of performance.

4. Conclusion and perspectives

This comprehensive review summarises the effectiveness of the strategies to reduce TEC values of SOFC cathodes. The aim is to achieve sustainable and efficient SOFCs by reducing the TEC values of the cathode while maintaining high electrochemical performance. While there have been promising developments in tailoring TEC values through the addition of specific elements and composite materials, as

Table 2
TEC values of electrodes using different strategies.

Type of strategy	Composition	TEC (10^{-6} K^{-1})		References
A-site substitution by lanthanides/elimination of cobalt	$La_{0.3}Sr_{0.7}Fe_{0.7}Cr_{0.3}O_{3-\delta}$	14.6 (40–580 °C)	20.2 (580–1000 °C)	[58]
	$Pr_{0.3}Sr_{0.7}Fe_{0.7}Cr_{0.3}O_{3-\delta}$	14.5 (40–600 °C)	19.1 (600–1000 °C)	[58]
	$Nd_{0.3}Sr_{0.7}Fe_{0.7}Cr_{0.3}O_{3-\delta}$	13.7 (40–630 °C)	20.3 (630–1000 °C)	[58]
	$Sm_{0.3}Sr_{0.7}Fe_{0.7}Cr_{0.3}O_{3-\delta}$	12.7 (40–640 °C)	19.5 (640–1000 °C)	[58]
Strontium substitution by barium	$Ba_{0.3}Sr_{0.7}Co_{0.8}Fe_{0.2}O_{3-\delta}$	28.74 (500–700 °C)	25.98 (500–1000 °C)	[59]
	$Ba_{0.4}Sr_{0.6}Co_{0.8}Fe_{0.2}O_{3-\delta}$	26.87 (500–700 °C)	25.38 (500–1000 °C)	[59]
	$Ba_{0.5}Sr_{0.5}Co_{0.8}Fe_{0.2}O_{3-\delta}$	24.95 (500–700 °C)	24.26 (500–1000 °C)	[59]
	$Ba_{0.6}Sr_{0.4}Co_{0.8}Fe_{0.2}O_{3-\delta}$	24.57 (500–700 °C)	23.80 (500–1000 °C)	[59]
	$Ba_{0.7}Sr_{0.3}Co_{0.8}Fe_{0.2}O_{3-\delta}$	23.79 (500–700 °C)	23.98 (500–1000 °C)	[59]
Strontium substitution by lanthanum	$La_{0.3}Sr_{0.7}CoO_{3-\delta}$	25 (30–1000 °C)	–	[113]
	$La_{0.5}Sr_{0.5}CoO_{3-\delta}$	22.3 (30–1000 °C)	–	[113]
	$La_{0.6}Sr_{0.4}CoO_{3-\delta}$	20.5 (30–1000 °C)	–	[113]
Cobalt elimination	$La_{0.6}Sr_{0.4}FeO_{3-\delta}$	16.3 (30–1000 °C)	–	[114]
Cobalt substitution by iron	$La_{0.6}Sr_{0.4}Fe_{0.8}Co_{0.2}O_3$	17.5 (30–1000 °C)	–	[113]
	$La_{0.6}Sr_{0.4}Fe_{0.5}Co_{0.5}O_3$	20.3 (30–1000 °C)	–	[78]
	$La_{0.6}Sr_{0.4}Fe_{0.2}Co_{0.8}O_3$	21.4 (30–1000 °C)	–	[78]
Strontium substitution by lanthanum and cobalt substitution by iron	$La_{0.8}Sr_{0.2}Fe_{0.9}Co_{0.1}O_{3-\delta}$	13.9 (30–1000 °C)	–	[113]
	$La_{0.8}Sr_{0.2}Fe_{0.8}Co_{0.2}O_{3-\delta}$	14.8 (30–1000 °C)	–	[113]
	$La_{0.8}Sr_{0.2}Fe_{0.2}Co_{0.8}O_{3-\delta}$	19.3 (30–1000 °C)	–	[78]
	$La_{0.8}Sr_{0.2}Fe_{0.5}Co_{0.5}O_{3-\delta}$	17.6 (30–1000 °C)	–	[78]
Strontium substitution by Praseodymium and cobalt substitution by iron and manganese	$Pr_{0.8}Sr_{0.2}Fe_{0.8}Co_{0.2}O_{3-\delta}$	12.8 (30–1000 °C)	–	[113]
	$Pr_{0.8}Sr_{0.2}Mn_{0.8}Co_{0.2}O_{3-\delta}$	10.9 (30–1000 °C)	–	[113]
Cobalt substitution by zirconium	$BaCo_{0.2}Zr_{0.8}O_{3-\delta}$	8.39 (50–800 °C)	–	[69]
	$BaCo_{0.4}Zr_{0.6}O_{3-\delta}$	11.12 (50–800 °C)	–	[69]
	$BaCo_{0.5}Zr_{0.5}O_{3-\delta}$	12.10 (50–800 °C)	–	[69]
	$BaCo_{0.6}Zr_{0.4}O_{3-\delta}$	12.60 (50–800 °C)	–	[69]
	$BaCo_{0.8}Zr_{0.2}O_{3-\delta}$	14.65 (50–800 °C)	–	[69]
A-site deficiency creation	$Pr_{0.65}Sr_{0.3}MnO_{3-\delta}$	11.6 (30–1000 °C)	–	[113]
	$Pr_{0.7}Sr_{0.3}Mn_{0.8}Co_{0.2}O_{3-\delta}$	11.1 (30–1000 °C)	–	[113]
	$Pr_{0.75}Sr_{0.2}Mn_{0.8}Co_{0.2}O_{3-\delta}$	10.8 (30–1000 °C)	–	[113]
	$La_{0.65}Sr_{0.3}Fe_{0.8}Co_{0.2}O_{3-\delta}$	14.9 (30–1000 °C)	–	[113]
	$(Ba_{0.5}Sr_{0.5})_1$ $Co_{0.8}Fe_{0.2}O_{3-\delta}$	14.4 (50–400 °C)	27.5 (450–700 °C)	[89]
	$(Ba_{0.5}Sr_{0.5})_{0.97}$ $Co_{0.8}Fe_{0.2}O_{3-\delta}$	11.9 (50–400 °C)	22.7 (450–700 °C)	[89]
	$(Ba_{0.5}Sr_{0.5})_{0.91}$ $Co_{0.8}Fe_{0.2}O_{3-\delta}$	12.3 (50–400 °C)	18.3 (450–700 °C)	[89]
	$(Ba_{0.5}Sr_{0.5})_{0.85}$ $Co_{0.8}Fe_{0.2}O_{3-\delta}$	12.1 (50–400 °C)	14.9 (450–700 °C)	[89]
	$(Ba_{0.5}Sr_{0.5})_{0.8}$ $Co_{0.8}Fe_{0.2}O_{3-\delta}$	9.5 (50–400 °C)	9.3 (450–700 °C)	[89]
Tuning electrolyte content in composite cathode	BSCN-(0% GDC)	16.2		[101]
	BSCN-(10% GDC)	15.5		[101]
	BSCN-(20% GDC)	14.9		[101]
	BSCN-(30% GDC)	14.6		[101]
	BSCN-(40% GDC)	13.5		[101]
	GSC-(0% SDC)	24.84		[51]
	GSC-(10% SDC)	23.35		[51]
	GSC-(20% SDC)	19.87		[51]
	GSC-(30% SDC)	16.74		[51]
	GSC-(40% SDC)	14.35		[51]
	GSC-(50% SDC)	13.38		[51]
	PBC	23.8 (30–900 °C)		[115]
	80% PBC-20% SDC	21.3 (30–900 °C)		[115]
	50%PBC-50% SDC	17.9 (30–900 °C)		[115]
Addition of NTE material into cathode material	SNC	20.5		[48]
	SNC-10%YWO	15.9		[48]
	SNC-20%YWO	12.9		[48]
	SNC-30%YWO	8.88		[48]
	SNC-40%YWO	5.99		[48]
	SNC-50%YWO	4.59		[48]

can be seen in the results summarised in Table 2, further research is needed to identify innovative strategies and novel materials. This requires a multidisciplinary approach, bringing together experts from various fields to address the challenge of reducing TEC values while optimizing performance.

There has been significant research towards achieving durability in Solid Oxide Fuel Cells (SOFCs), but a major issue concerning delamination remains unresolved. The cathode layer is responsible for producing the high overpotential in SOFCs at lower temperatures that offsets benefit in durability, making it crucial to focus on developing a new cathode material that can optimize performance and durability at intermediate temperatures, while also meeting performance, cost, and durability goals. Lowering the operating temperature can enhance chemical and thermo-mechanical stability, but it can also create challenges in overall ORR activity and lead to performance loss. Several cathodes, such as BSCF, LSCF, SSNC, SSTC, and SCNT, perform exceptionally well electrochemically at intermediate temperatures, but they fail to provide long-term stable output due to thermo-mechanical incompatibility with commonly used electrolytes such as YSZ, SDC, GDC, and LSGM. This incompatibility primarily stems from the high thermal expansion coefficient of the promising cathode materials, which can cause mechanical failure of the cell in the long run and result in unreliable performance.

Perovskite type materials that are commonly utilized in SOFC have a crucial combination of mixed ionic and electronic conductivity, which is an essential requirement for high performing cathode material. The crystalline structure of the perovskite material is also important, with most studies concluding that the cubic structure of the perovskite material is optimal for electrochemical activity. Strontium cobaltite is a popular perovskite material used as the parent oxide for energy-generating devices due to its favourable electronic conductivity and power density. However, the practical use of this type of cathode is hindered by its phase instability below 900 °C and higher TEC. Another potential material are double perovskite materials, but these cathodes are also having a high TEC value (more than $20*10^{-6}$ K^{-6}). Double perovskites have rock salt type ordered arrangements such as $A_2BB'O_6$, $AA'B_2O_6$, or $AA'BB'O_6$, where A, A′, B, and B′ elements are all different. A-site cations are typically alkali, alkaline earth, or rare-earth ions, while B-site cations are transition metal ions. These materials are extensively studied due to their capacity to hold large amounts of oxygen non-stoichiometry. Considering the efficacy of these materials and their limitations due to the higher TEC value, the following strategies aim to balance TEC reduction with maintaining electrochemical performance, offering potential solutions to the persistent challenge of cathode delamination.

4.1. Material development

This section explores strategies to address the challenge of delamination arising from the higher TEC of cathodes, proposing solutions such as A-site and/or B-site substitution, A-site deficiency creation, electrolyte addition, and NTE incorporation. The paper suggests combining these strategies, introducing composite cathodes with optimized combinations of NTE materials and electrolytes to achieve a balance between TEC reduction and electrochemical performance. The potential impact of NTE addition on cell performance is discussed, along with examples of NTE materials and their TEC values. The strategy of A-site and/or B-site substitution in strontium cobaltite (SC)-based perovskites could be useful. However, the presence of strontium and cobalt is correlated with higher electrochemical performance, and the complete elimination of these elements may pose challenges to performance. Strategies like A-site deficiency creation, electrolyte addition, and negative thermal expansion (NTE) addition into the base perovskite structure have their limits, as they can interfere with cubic symmetry, porosity, and impurity formation.

Combining two strategies may overcome these limitations and produce a synergistic effect. For instance, creating composite structures by adding a compatible electrolyte phase to the existing cathode can tailor TEC and achieve a linear TEC profile when the electrolyte used has a linear TEC profile. Further reduction in TEC can be accomplished by adding NTE material to the composition. In this three-phase composite cathode, electrolyte addition extends the triple-phase boundary (TPB) and helps attain a linear TEC profile, while NTE addition contributes more towards TEC reduction. Multi-phase composite cathodes with an optimum quantity of NTE and electrolyte could be a useful strategy to maintain high-performance electrochemical activity after numerous thermal cycles.

NTE addition is a new approach for reducing the TEC of the cathode, but it may produce another phase in the composition that can disturb the overall performance of the cell. A few examples of NTE materials that can be used to produce a composite cathode are presented in Table 3. These materials are selected due to their phase stability at operating temperature, isometric behaviour, and negative value of thermal expansion. YWO is preferable due to its phase stability and easy fabrication, but ZrW_2O_8 (ZWO) produced using the hydrothermal method may also be of interest. Cost is an important commercialization factor, and the cost of scandium raw material may limit the use of $Sc_2W_3O_{12}$ (SWO) to provide a feasible solution. If NTE addition impacts electrochemical behaviour, the ionic conductivity of NTE can be increased by strategically doping the NTE material to improve the overall conductivity of the composite cathode. Another combination can be producing a composite cathode using A and/or B site substituted cathode having A-site deficiency mixed in a composite structure with NTE material to further reduce TEC and find the optimum solution. The combination of these strategies can provide a feasible solution to the challenge of delamination caused by higher TEC of the cathode, and further research is needed to optimize the properties of the composite cathode.

4.2. Characterization techniques

In the pursuit of optimal performance and practical application of SOFCs, understanding the interplay among different components is crucial. This section explores advanced analytical techniques such as Focused Ion Beam Scanning Electron Microscopy (FIB-SEM) for delamination analysis, X-ray diffraction (XRD) challenges in composite cathodes, and the integration of high-resolution transmission electron microscopy (HRTEM) and energy-dispersive X-ray spectroscopy (EDS) mapping for comprehensive composite cathode characterization.

Scanning Electron Microscopy (SEM) is a powerful tool for scrutinizing SOFC cathodes in terms of microstructure, such as grain sizes, composite phase dispersion, and pore structure. However, SEM has inherent limitations when it comes to the delamination analysis. A primary concern revolves around the potential for sample cracking during SEM sample preparation that cannot be distinguished from delamination during cell operation. This ambiguity can significantly impact the overall conclusions drawn from the delamination analysis.

In this context, Focused Ion Beam (FIB) SEM emerges as a powerful tool offering distinct advantages over traditional SEM methods. FIB SEM facilitates layer-by-layer analysis without compromising the surface of the cross-section, making it an excellent tool for precise and non-destructive analysis of delamination in SOFC. By combining SEM and FIB in 3D imaging, a more comprehensive understanding of delamination processes can be achieved. Fig. 8a and b presents typical analysis examples demonstrating the capability to observe and characterize

Table 3
Suggested NTE materials and their average TEC values.

NTE materials	TEC ($*10^{-6}$ K^{-1})	Operating-Temperature (°C)	References
α-ZrW_2O_8	−9	<152	[116]
β-ZrW_2O_8	−6	152–777	[116]
$Sc_2W_3O_{12}$	−11	RT – 927	[117]
$Y_2W_3O_{12}$	−7	−258 – 1100	[118]

delamination and its impact in a three-dimensional view.

X-ray diffraction (XRD) analysis stands as a widely employed technique for exploring the crystal structure of materials. Nevertheless, when applied to composite cathode materials—comprising elements like perovskite, electrolyte, and NTE components to finely tune the cathode's TEC, XRD encounters several limitations. The sensitivity of XRD analysis is inherently constrained by the quantity of material present in the sample. Composite cathodes often exhibit intricate structures with multiple phases and diverse crystallographic orientations, posing challenges for accurate analysis. The meticulous preparation of heterogeneous composite cathode samples further complicates the reliable application of XRD.

In addressing these challenges, high-resolution transmission electron microscopy (HRTEM) and energy-dispersive X-ray spectroscopy (EDS) mapping emerge as complementary techniques capable of overcoming the limitations of XRD analysis in composite cathodes. HRTEM analysis facilitates a granular understanding of the microstructure of composite cathodes, offering insights into the identification of individual components and phases within the material. Concurrently, EDS mapping aids in determining the chemical composition and the spatial distribution of elements within the composite material. The integration of XRD, HRTEM, and EDS mapping yields a comprehensive characterization, as illustrated in Fig. 8c, providing a detailed depiction of the microstructure and composition of composite cathodes. This multifaceted approach enriches our understanding of the properties and behaviour of composite cathodes within SOFCs.

Electrochemical stability testing is an important part of the development and optimization of SOFCs, as it allows for the evaluation of the long-term performance and durability of the cathodes under operating conditions. However, this test is time-consuming, typically needing extended periods of operation under steady-state, power cycling, or thermal cycling conditions, which can take months to complete. This can make it difficult to evaluate many materials or configurations or to make rapid progress in the development of new SOFC technologies. Particularly in the case of observing the impact of thermal expansion mismatch, it is not possible to observe in a few weeks. This limitation can be overcome by accelerating the degradation process, which can be achieved for delamination by using rapid thermal cycling tests, where frequent thermal cycles can cause measurable delamination after a certain number of thermal cycles.

Also, stability testing is typically performed on small-scale SOFCs, which may not accurately reflect the thermal gradients, stress levels, performance, or mechanical behaviour of larger, commercial-scale cells. This can make it difficult to extrapolate stability data to real-world applications or to optimize the design of large-scale SOFC systems. To overcome this limitation, a testing tool needs to be designed using modelling and simulation for optimizing and better understanding the stability of materials used in SOFC.

4.3. TEC with other challenges

In the pursuit of advancing SOFC technology, it is imperative to not only address specific challenges but also ensure that proposed strategies align harmoniously with the goal of achieving optimal electrochemical activity. While various strategies have been proposed to address specific challenges, it is important not to compromise the goal of achieving high electrochemical activity. For instance, substituting strontium and cobalt to reduce the TEC may come at the expense of reduced electrochemical activity. To address this issue, incorporating electrolyte or negative thermal expansion (NTE) into the cathode material has been suggested as a potential solution. However, it is crucial to determine the appropriate amount of electrolyte or NTE that can be added to optimize the TEC value and ORR activity of the cathode, as excess addition may interfere with the crystal structure required for high MIEC properties. Achieving structural stability under operating conditions and performing molecular-level analysis are critical components of successful SOFC development.

To compare a new cathode material's ORR performance with the base material, distribution of relaxation time (DRT) analysis can be a useful technique. DRT analysis, when coupled with Electrochemical Impedance Spectroscopy (EIS), provides a comprehensive understanding of the ORR stages in cathode materials. EIS captures impedance data across different frequencies, and DRT analysis dissects this complex spectrum. This technique deconvolutes the electrochemical impedance spectroscopy (EIS) data and provides more information on each step involved in the complex ORR, typically classified into low, intermediate, and high-frequency regions [121,122]. Low-frequency peaks are associated with mass transfer [123], while intermediate frequency peaks are associated with the dissociation of O_2 to $2O_{ads}$ [124–126], and high-frequency peaks are associated with the diffusion of O^{-2} [127]. It is an integral technique to have a fair comparison between two materials as they enable a comprehensive evaluation of each step that can significantly impact performance and differentiate them from one another.

In conclusion, while each strategy has its own advantages, the goal of achieving optimal electrochemical activity needs to be balanced. It is essential to carefully consider the impact of each component on the overall system and conduct thorough analysis and testing to ensure that the resulting SOFC meets the requirements for stability, durability, and electrochemical activity needed for commercialization.

CRediT authorship contribution statement

Nilam Shah: Writing – review & editing, Writing – original draft, Methodology, Investigation, Data curation, Conceptualization. **Xiaoyong Xu:** Writing – review & editing, Supervision, Conceptualization. **Jonathan Love:** Writing – review & editing, Data curation. **Hao Wang:** Writing – original draft, Methodology. **Zhonghua Zhu:** Writing –

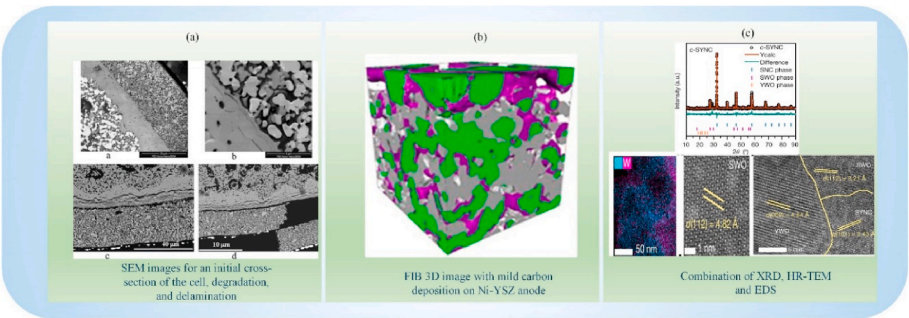

Fig. 8. (a) SEM images for an initial cross-section of the cell, degradation, and delamination Reproduced with permission [119]. Copyright 2011, Elsevier. (b) FIB 3D image with mild carbon deposition on Ni-YSZ anode Reproduced with permission [120]. Copyright 2023, Elsevier. (c) Combination of XRD, HR-TEM, and EDS Reproduced with permission [48]. Copyright 2021, Springer Nature.

review & editing, Writing – original draft, Supervision, Funding acquisition, Conceptualization. **Lei Ge:** Writing – review & editing, Writing – original draft, Supervision, Project administration, Methodology, Funding acquisition, Conceptualization.

Declaration of competing interest

The authors declare that they have no known competing financial interests or personal relationships that could have appeared to influence the work reported in this paper.

Data availability

Data will be made available on request.

Acknowledgement

N Shah would like to thank the RTP research scholarship from the University of Queensland. ZH Zhu and H Wang would like to thank the financial support from Australian Research Council Discovery Project DP190101782. L Ge wants to thank the financial support from ARC Future Fellowship project FT220100166.

References

[1] A.B. Stambouli, E. Traversa, Renew. Sustain. Energy Rev. 6 (2002) 433–455.
[2] M.C. Williams, J.P. Strakey, W.A. Surdoval, J. Power Sources 143 (2005) 191–196.
[3] M.S. Khan, X. Xu, R. Knibbe, A.u. Rehman, Z. Li, A.J. Yago, H. Wang, Z. Zhu, Energy Technol. 8 (2020) 2000241.
[4] D.J.L. Brett, A. Atkinson, N.P. Brandon, S.J. Skinner, Chem. Soc. Rev. 37 (2008) 1568–1578.
[5] B.C.H. Steele, A. Heinzel, Nature 414 (2001) 345–352.
[6] R.M. Ormerod, Chem. Soc. Rev. 32 (2003) 17–28.
[7] M. Wang, C. Su, Z. Zhu, H. Wang, L. Ge, Compos. B Eng. 238 (2022) 109881.
[8] E. Maguire, B. Gharbage, F.M.B. Marques, J.A. Labrincha, Solid State Ionics 127 (2000) 329–335.
[9] J. Li, X. Zhou, C. Wu, L. Zhao, B. Dong, S. Wang, B. Chi, Chem. Eng. J. 438 (2022) 135446.
[10] J.M. Vohs, R.J. Gorte, Adv. Mater. 21 (2009) 943–956.
[11] D. Ding, X. Li, S.Y. Lai, K. Gerdes, M. Liu, Energy Environ. Sci. 7 (2014) 552–575.
[12] M. Zhang, G. Jeerh, P. Zou, R. Lan, M. Wang, H. Wang, S. Tao, Mater. Today 49 (2021) 351–377.
[13] S.K. Burnwal, S. Bharadwaj, P. Kistaiah, Journal of Molecular and Engineering Materials 4 (2016) 1630001.
[14] Z. Li, M. Li, Z. Zhu, Electrochem. Energy Rev. 5 (2022) 263–311.
[15] M.Y. Lu, J.G. Railsback, H. Wang, Q. Liu, Y.A. Chart, S.-L. Zhang, S.A. Barnett, J. Mater. Chem. A 7 (2019) 13531–13539.
[16] W. Zhang, H. Wang, K. Guan, Z. Wei, X. Zhang, J. Meng, X. Liu, J. Meng, ACS Appl. Mater. Interfaces 11 (2019) 26830–26841.
[17] H. Chen, Z. Guo, L.A. Zhang, Y. Li, F. Li, Y. Zhang, Y. Chen, X. Wang, B. Yu, J.-m. Shi, J. Liu, C. Yang, S. Cheng, Y. Chen, M. Liu, ACS Appl. Mater. Interfaces 10 (2018) 39785–39793.
[18] Z. Shao, S.M. Haile, Nature 431 (2004) 170–173.
[19] C. Su, X. Xu, Y. Chen, Y. Liu, M.O. Tadé, Z. Shao, J. Power Sources 274 (2015) 1024–1033.
[20] M. Li, M. Zhao, F. Li, W. Zhou, V.K. Peterson, X. Xu, Z. Shao, I. Gentle, Z. Zhu, Nat. Commun. 8 (2017) 13990.
[21] X. Xu, J. Zhao, M. Li, L. Zhuang, J. Zhang, S. Aruliah, F. Liang, H. Wang, Z. Zhu, Compos. B Eng. 178 (2019) 107491.
[22] X. Mao, Z. Li, M. Li, X. Xu, C. Yan, Z. Zhu, A. Du, J. Am. Chem. Soc. 143 (2021) 9507–9514.
[23] W. Jia, Z. Huang, W. Sun, L. Wu, L. Zheng, Y. Wang, J. Huang, X. Yang, M. Lv, L. Ge, J. Power Sources 490 (2021) 229564.
[24] H. Gu, M. Xu, Y. Song, C. Zhou, C. Su, W. Wang, R. Ran, W. Zhou, Z. Shao, Compos. B Eng. 213 (2021) 108726.
[25] W. Zhou, W. Jin, Z. Zhu, Z. Shao, Int. J. Hydrogen Energy 35 (2010) 1356–1366.
[26] H. Kruidhof, H.J.M. Bouwmeester, R.H.E.v. Doorn, A.J. Burggraaf, Solid State Ionics 63–65 (1993) 816–822.
[27] M. Li, W. Zhou, Z. Zhu, Asia Pac. J. Chem. Eng. 11 (2016) 370–381.
[28] R. Vinoth Kumar, A.P. Khandale, Renew. Sustain. Energy Rev. 156 (2022) 111985.
[29] Z. Yang, M. Guo, N. Wang, C. Ma, J. Wang, M. Han, Int. J. Hydrogen Energy 42 (2017) 24948–24959.
[30] P. Kaur, K. Singh, Ceram. Int. 46 (2020) 5521–5535.
[31] F. Wang, H. Kishimoto, T. Ishiyama, K. Develos-Bagarinao, K. Yamaji, T. Horita, H. Yokokawa, J. Power Sources 478 (2020) 228763.
[32] A.I. Klyndyuk, E.A. Chizhova, D.S. Kharytonau, D.A. Medvedev, Materials 15 (2022) 141.
[33] R. Pelosato, G. Cordaro, D. Stucchi, C. Cristiani, G. Dotelli, J. Power Sources 298 (2015) 46–67.
[34] A.V. Nikonov, K. Kuterbekov, K.Z. Bekmyrza, N.B. Pavzderin, Eurasian Journal of Physics and Functional Materials 2 (2018) 274–292.
[35] C. Sun, R. Hui, J. Roller, J. Solid State Electrochem. 14 (2010) 1125–1144.
[36] A. Jun, J. Kim, J. Shin, G. Kim, Chemelectrochem 3 (2016) 511–530.
[37] S.P. Jiang, J. Mater. Sci. 43 (2008) 6799–6833.
[38] C.M. Harrison, P.R. Slater, R. Steinberger-Wilckens, Solid State Ionics 354 (2020) 115410.
[39] L. Zhou, J.H. Mason, W. Li, X. Liu, Renew. Sustain. Energy Rev. 134 (2020) 110320.
[40] Y. Chen, W. Zhou, D. Ding, M. Liu, F. Ciucci, M. Tade, Z. Shao, Adv. Energy Mater. 5 (2015) 1500537.
[41] J. Richter, P. Holtappels, T. Graule, T. Nakamura, L.J. Gauckler, Monatshefte für Chemie - Chemical Monthly 140 (2009) 985–999.
[42] M.Z. Ahmad, S.H. Ahmad, R.S. Chen, A.F. Ismail, R. Hazan, N.A. Baharuddin, Int. J. Hydrogen Energy 47 (2022) 1103–1120.
[43] A. Elamiri, A. Saifi, O. Abdellatif, Y. Errami, S. Smail, A. Elhassnaoui, Control of Solid Oxide Fuel Cells Damage Using Infrared Thermography, 2017.
[44] K. Park, S. Yu, J. Bae, H. Kim, Y. Ko, Int. J. Hydrogen Energy 35 (2010) 8670–8677.
[45] B. Wei, Z. Lu, S. Li, Y. Liu, K. Liu, W. Su, Electrochem. Solid State Lett. 8 (2005) A428.
[46] S. Wang, M. Katsuki, M. Dokiya, T. Hashimoto, Solid State Ionics 159 (2003) 71–78.
[47] L.W. Tai, M.M. Nasrallah, H.U. Anderson, D.M. Sparlin, S.R. Sehlin, Solid State Ionics 76 (1995) 273–283.
[48] Y. Zhang, B. Chen, D. Guan, M. Xu, R. Ran, M. Ni, W. Zhou, R. O'Hayre, Z. Shao, Nature 591 (2021) 246–251.
[49] W. Zhou, J. Sunarso, M. Zhao, F. Liang, T. Klande, A. Feldhoff, Angew. Chem. Int. Ed. 52 (2013) 14036–14040.
[50] B. Gu, J. Sunarso, Y. Zhang, Y. Song, G. Yang, W. Zhou, Z. Shao, J. Power Sources 405 (2018) 124–131.
[51] Y. Ji, H. Wang, H. Zhang, Mater. Res. Bull. 85 (2017) 30–34.
[52] E.V. Tsipis, V.V. Kharton, J. Solid State Electrochem. 12 (2008) 1367–1391.
[53] R.J. Tilley, Perovskites: Structure-Property Relationships, John Wiley & Sons, 2016.
[54] S.Y. Istomin, O.A. Drozhzhin, P.S. Napolsky, S.N. Putilin, A.A. Gippius, E. V. Antipov, Solid State Ionics 179 (2008) 1054–1057.
[55] J. Kim, S. Choi, A. Jun, H.Y. Jeong, J. Shin, G. Kim, ChemSusChem 7 (2014) 1669–1675.
[56] W. Zhang, L. Zhang, K. Guan, X. Zhang, J. Meng, H. Wang, X. Liu, J. Meng, J. Power Sources 446 (2020) 227360.
[57] J.H. Kim, S.-W. Baek, C. Lee, K. Park, J. Bae, Solid State Ionics 179 (2008) 1490–1496.
[58] L. Lin, Q. Xu, Y.-P. Wang, M. Chen, J. Xiao, D.-P. Huang, F. Zhang, Mater. Res. Bull. 106 (2018) 263–270.
[59] B. Wei, Z. Lü, X. Huang, J. Miao, X. Sha, X. Xin, W. Su, J. Eur. Ceram. Soc. 26 (2006) 2827–2832.
[60] T. Nagai, W. Ito, T. Sakon, Solid State Ionics 177 (2007) 3433–3444.
[61] A.J. Fernández-Ropero, J.M. Porras-Vázquez, A. Cabeza, P.R. Slater, D. Marrero-López, E.R. Losilla, J. Power Sources 249 (2014) 405–413.
[62] S. Park, S. Choi, J. Shin, G. Kim, Electrochim. Acta 125 (2014) 683–690.
[63] M. Li, M. Zhao, F. Li, W. Zhou, V.K. Peterson, X. Xu, Z. Shao, I. Gentle, Z. Zhu, Nat. Commun. 8 (2017) 13990.
[64] J.A. Kilner, R.J. Brook, Solid State Ionics 6 (1982) 237–252.
[65] A.F. Sammells, R.L. Cook, J.H. White, J.J. Osborne, R.C. MacDuff, Solid State Ionics 52 (1992) 111–123.
[66] L. Zhao, J. Shen, B. He, F. Chen, C. Xia, Int. J. Hydrogen Energy 36 (2011) 3658–3665.
[67] Y. Lu, H. Zhao, X. Chang, X. Du, K. Li, Y. Ma, S. Yi, Z. Du, K. Zheng, K. Świerczek, J. Mater. Chem. A 4 (2016) 10454–10466.
[68] L.-W.F. Tai, M.M. Nasrallah, H.U. Anderson, D.M. Sparlin, S.R. Sehlin, Solid State Ionics 76 (1995) 259–271.
[69] H. Qi, T. Zhang, M. Cheng, D. Liu, B. Tu, J. Eur. Ceram. Soc. 42 (2022) 1042–1052.
[70] L. Qiu, T. Ichikawa, A. Hirano, N. Imanishi, Y. Takeda, Solid State Ionics 158 (2003) 55–65.
[71] Z. Chen, R. Ran, W. Zhou, Z. Shao, S. Liu, Electrochim. Acta 52 (2007) 7343–7351.
[72] H. Lv, B.-Y. Zhao, Y.-J. Wu, G. Sun, G. Chen, K.-A. Hu, Mater. Res. Bull. 42 (2007) 1999–2012.
[73] E. Olsson, J. Cottom, X. Aparicio-Anglès, N.H. de Leeuw, Phys. Chem. Chem. Phys. 21 (2019) 9407–9418.
[74] S. Joo, J. Kim, J. Shin, T.-H. Lim, G. Kim, J. Electrochem. Soc. 163 (2016) F1489.
[75] L. Tong, D. Tian, IOP Conf. Ser. Mater. Sci. Eng. 490 (2019) 022029.
[76] G. Zhang, X. Dong, Z. Liu, W. Zhou, Z. Shao, W. Jin, J. Power Sources 195 (2010) 3386–3393.
[77] W. Jia, Y. Wang, J. Huang, M. Li, B. Xiang, Y. Wang, L. Wu, L. Zheng, L. Ge, Appl. Energy 353 (2024) 122096.
[78] G.C. Kostogloudis, C. Ftikos, Solid State Ionics 126 (1999) 143–151.
[79] A. Mineshige, J. Izutsu, M. Nakamura, K. Nigaki, J. Abe, M. Kobune, S. Fujii, T. Yazawa, Solid State Ionics 176 (2005) 1145–1149.
[80] K.K. Hansen, K.V. Hansen, Solid State Ionics 178 (2007) 1379–1384.

[81] D. Neagu, G. Tsekouras, D.N. Miller, H. Ménard, J.T.S. Irvine, Nat. Chem. 5 (2013) 916–923.
[82] Y. Sun, J. Li, Y. Zeng, B.S. Amirkhiz, M. Wang, Y. Behnamian, J. Luo, J. Mater. Chem. A 3 (2015) 11048–11056.
[83] G. Tsekouras, D. Neagu, J.T.S. Irvine, Energy Environ. Sci. 6 (2013) 256–266.
[84] H. Kim, C. Lim, O. Kwon, J. Oh, M.T. Curnan, H.Y. Jeong, S. Choi, J.W. Han, G. Kim, Nat. Commun. 12 (2021) 6814.
[85] Y. Gao, D. Chen, M. Saccoccio, Z. Lu, F. Ciucci, Nano Energy 27 (2016) 499–508.
[86] K.J. Kim, H. Han, T. Defferriere, D. Yoon, S. Na, S.J. Kim, A.M. Dayaghi, J. Son, T.-S. Oh, H.M. Jang, G.M. Choi, J. Am. Chem. Soc. 141 (2019) 7509–7517.
[87] Z. Liu, L.-z. Cheng, M.-F. Han, J. Power Sources 196 (2011) 868–871.
[88] Z.-B. Yang, M.-F. Han, P. Zhu, F. Zhao, F. Chen, Int. J. Hydrogen Energy 36 (2011) 9162–9168.
[89] W. Zhou, R. Ran, Z. Shao, W. Jin, N. Xu, J. Power Sources 182 (2008) 24–31.
[90] G. Kim, S. Wang, A.J. Jacobson, L. Reimus, P. Brodersen, C.A. Mims, J. Mater. Chem. 17 (2007) 2500–2505.
[91] K. Zhang, L. Ge, R. Ran, Z. Shao, S. Liu, Acta Mater. 56 (2008) 4876–4889.
[92] D. Chen, R. Ran, K. Zhang, J. Wang, Z. Shao, J. Power Sources 188 (2009) 96–105.
[93] Q. Zhou, F. Wang, Y. Shen, T. He, J. Power Sources 195 (2010) 2174–2181.
[94] S. Pang, X. Jiang, X. Li, Q. Wang, Z. Su, J. Power Sources 204 (2012) 53–59.
[95] S.L. Pang, X.N. Jiang, X.N. Li, H.X. Xu, L. Jiang, Q.L. Xu, Y.C. Shi, Q.Y. Zhang, J. Power Sources 240 (2013) 54–59.
[96] X. Jiang, Y. Shi, W. Zhou, X. Li, Z. Su, S. Pang, L. Jiang, J. Power Sources 272 (2014) 371–377.
[97] X. Jiang, Q. Xu, Y. Shi, X. Li, W. Zhou, H. Xu, Q. Zhang, Int. J. Hydrogen Energy 39 (2014) 10817–10823.
[98] I.D. Seymour, A. Chroneos, J.A. Kilner, R.W. Grimes, Phys. Chem. Chem. Phys. 13 (2011) 15305–15310.
[99] M. Juhl, S. Primdahl, C. Manon, M. Mogensen, J. Power Sources 61 (1996) 173–181.
[100] W.H. Kan, A.J. Samson, V. Thangadurai, J. Mater. Chem. A 4 (2016) 17913–17932.
[101] L. Zhang, M. Liu, J. Huang, Z. Song, Y. Fu, Y. Chang, C. Li, T. He, Int. J. Hydrogen Energy 39 (2014) 7972–7979.
[102] P. Hjalmarsson, M. Mogensen, J. Power Sources 196 (2011) 7237–7244.
[103] A.J. Abd Aziz, N.A. Baharuddin, M.R. Somalu, A. Muchtar, Ceram. Int. 46 (2020) 23314–23325.
[104] Y. Leng, S.H. Chan, Q. Liu, Int. J. Hydrogen Energy 33 (2008) 3808–3817.
[105] Y. Leng, S. Chan, S. Jiang, K. Khor, Solid State Ionics 170 (2004) 9–15.
[106] C. Fu, K. Sun, N. Zhang, X. Chen, D. Zhou, Electrochim. Acta 52 (2007) 4589–4594.
[107] S. Lee, H.S. Song, S.H. Hyun, J. Kim, J. Moon, J. Power Sources 195 (2010) 118–123.
[108] D. Heidari, S. Javadpour, S.H. Chan, Energy Convers. Manag. 136 (2017) 78–84.
[109] K. Wang, R. Ran, W. Zhou, H. Gu, Z. Shao, J. Ahn, Journal of Power Sources - J POWER SOURCES 179 (2008) 60–68.
[110] K. Takenaka, Sci. Technol. Adv. Mater. 13 (2012) 013001.
[111] F. Lu, M. Yang, Y. Shi, C. Wu, X. Jia, H. He, J. Su, M. Chao, B. Cai, Ceram. Int. 47 (2021) 1095–1100.
[112] L. Hu, D. Zhou, X. Zhu, N. Wang, J. Bai, H. Gong, Y. Zhang, Y. Chen, W. Yan, Q. Zhu, Fuel 362 (2024) 130864.
[113] H. Ullmann, N. Trofimenko, F. Tietz, D. Stöver, A. Ahmad-Khanlou, Solid State Ionics 138 (2000) 79–90.
[114] I. Yasuda, K. Ogasawara, M. Hishinuma, T. Kawada, M. Dokiya, Solid State Ionics 86–88 (1996) 1197–1201.
[115] D. Chen, R. Ran, Z. Shao, J. Power Sources 195 (2010) 7187–7195.
[116] J.S.O. Evans, T.A. Mary, T. Vogt, M.A. Subramanian, A.W. Sleight, Chem. Mater. 8 (1996) 2809–2823.
[117] J.S.O. Evans, T.A. Mary, A.W. Sleight, J. Solid State Chem. 137 (1998) 148–160.
[118] P.M. Forster, A.W. Sleight, Int. J. Inorg. Mater. 1 (1999) 123–127.
[119] M.A. Laguna-Bercero, R. Campana, A. Larrea, J.A. Kilner, V.M. Orera, J. Power Sources 196 (2011) 8942–8947.
[120] A. Sciazko, Y. Komatsu, A. Nakamura, Z. Ouyang, T. Hara, N. Shikazono, Chem. Eng. J. 460 (2023) 141680.
[121] Y. Chen, S. Yoo, Y. Choi, J.H. Kim, Y. Ding, K. Pei, R. Murphy, Y. Zhang, B. Zhao, W. Zhang, H. Chen, Y. Chen, W. Yuan, C. Yang, M. Liu, Energy Environ. Sci. 11 (2018) 2458–2466.
[122] Y. Chen, Y. Bu, Y. Zhang, R. Yan, D. Ding, B. Zhao, S. Yoo, D. Dang, R. Hu, C. Yang, M. Liu, Adv. Energy Mater. 7 (2017) 1601890.
[123] J.-D. Kim, G.-D. Kim, J.-W. Moon, Y.-i. Park, W.-H. Lee, K. Kobayashi, M. Nagai, C.-E. Kim, Solid State Ionics 143 (2001) 379–389.
[124] J. Wang, L. Jiang, X. Xiong, C. Zhang, X. Jin, L. Lei, K. Huang, J. Electrochem. Soc. 163 (2016) F891–F898.
[125] M. Li, Y. Ren, Z. Zhu, S. Zhu, F. Chen, Y. Zhang, C. Xia, Electrochim. Acta 191 (2016) 651–660.
[126] Z. Jiang, Z. Lei, B. Ding, C. Xia, F. Zhao, F. Chen, Int. J. Hydrogen Energy 35 (2010) 8322–8330.
[127] Y. Takeda, R. Kanno, M. Noda, Y. Tomida, O. Yamamoto, J. Electrochem. Soc. 134 (1987) 2656–2661.